NAZARBAYEV UNIVERSITY

ENHANCING EFFECTIVENESS OF OXIDATIVE DRUGS COMBINATION (ATO/D-VC) IN KRAS MUTANT COLORECTAL CANCER TREATMENT WITH PROTEASE-FUNCTIONALIZED NANOCARRIERS: A 2D AND 3D CELL CULTURE STUDY

ANEL MUN

(B.Sc., Nazarbayev University)

A THESIS SUBMITTED IN PARTIAL FULFILMENT OF THE REQUIREMENT OF NAZARBAYEV UNIVERSITY FOR THE DEGREE OF MASTER OF LIFE SCIENCES

APRIL 2025

Student: Anel Mun

Student's Supervisor: Prof. Dos Sarbassov

Student's Co-Supervisor: Prof. Vesselin Paunov

EXAMINERS

The M.Sc. thesis of Anel Mun has been approved by the examiners.

Prof. Gonzalo Hap Hortelano, PhD, School of Sciences and Humanities, Nazarbayev University

Prof. Marina Kriajevskaia, PhD, School of Medicine, Nazarbayev University

DECLARATION

I hereby declare that this thesis is my original work, and it has been written by my in its entirety.
I have duly acknowledged all the sources of information which have been used in the thesis.
This thesis has also not been submitted for any degree in any university previously.

Anel Mun

17 April 2025

ACKNOWLEDGMENTS

I would like to express my sincere gratitude to Professor Vesselin Paunov and Dr. Agata Burska for the invaluable opportunity to work on this project and for their continuous guidance, mentorship, and support throughout the research process.

I am also deeply thankful to Professor Dos Sarbassov, my official thesis supervisor, for his support and for his significant contribution to the development of the ATO/D-VC combination drug treatment.

Special thanks go to my labmate, Nuriya Nurlankyzy, for her tremendous assistance in the formulation and characterization of nanoparticles. I am also grateful to Saule Kalmagambetova, my lab colleague, for her support and help during experimental work.

To my dear friend, Zariat Shatkenova, thank you for being a strong and steady support system throughout this journey, and for your advice and encouragement during challenging moments.

I would also like to extend my heartfelt appreciation to my family and friends for their unconditional support and belief in me.

Finally, I thank the Core Facility technicians for their assistance with SEM imaging, which contributed significantly to the characterization part of this project.

TABLE OF CONTENTS

ABSTRACT

KRAS mutations are associated with treatment resistance and poor prognosis in colorectal cancer (CRC), highlighting the need for more effective therapeutic approaches. The combination of arsenic trioxide (ATO) and D-vitamin C (D-VC) has shown promise as an oxidative therapy that targets KRAS-mutant CRC cells by disrupting mitochondria and antioxidant defenses to trigger apoptosis. Although this combination has shown strong efficacy in 2D cell cultures, animal models, and early clinical trials, insight into its behavior in systems that closely replicate the structural features of the tumor microenvironment remains limited. Therefore, 3D *in vitro* models offer a valuable platform for bridging this gap.

This study evaluated the cytotoxicity of ATO/D-VC in 3D cell models known as clusteroids, derived from two KRAS-mutant CRC cell lines, HCT116 and SW620, and directly compared their response to corresponding 2D cultures. Clusteroids closely mimic key aspects of the tumor environment, including cell–cell interactions, extracellular matrix (ECM) deposition, and limited drug diffusion, offering a more predictive platform for assessing treatment efficacy. While ATO/D-VC showed a synergistic cytotoxic effect in 2D, the response in 3D clusteroids was significantly reduced, suggesting that drug access to inner cell layers was limited by ECM barriers.

To improve delivery, ATO and D-VC were individually encapsulated in shellac–poloxamer nanoparticles functionalized with Savinase, a protease known to degrade ECM components. These nanoparticles exhibited colloidal stability, a positive surface charge to enhance interaction with negatively charged cancer cells, and enzymatic activity to access cells in the core of 3D models. In clusteroids, co-delivery of the two nanoparticle formulations restored and enhanced the cytotoxic effect of ATO/D-VC, outperforming both free drug and uncoated formulations. This dual-nanoparticle approach preserved the synergistic interaction and led to a substantial reduction in viability and proliferation, particularly in CRC cells.

These results highlight the importance of 3D models in preclinical evaluation and demonstrate the potential of functionalized nanoparticles to enhance oxidative drug delivery in solid tumors.

LIST OF TABLES

LIST OF FIGURES AND ILLUSTRATIONS

ABBREVIATIONS

ATPS	aqueous two-phase system
ATO	arsenic trioxide
ATO/D-VC	combined treatment with arsenic trioxide and D-vitamin C
CRC	colorectal cancer
D-VC	D-form of Vitamin C
DEX	dextran
DHA	dehydroascorbate
DLS	dynamic light scattering
DMEM	Dulbecco's Modified Eagle Medium
DMEM/F12	mixture of DMEM and Ham's F-12 medium
ECM	extracellular matrix
FBS	fetal bovine serum
GSH	glutathione
KRAS	Kirsten Rat Sarcoma Viral Oncogene
NP/NPs	nanoparticle/nanoparticles
PBS	phosphate-buffered saline
PEO	poly (ethylene oxide)
PI	propidium iodide
ROS	reactive oxygen species
Sav	Savinase
Sav-ATO NPs	Savinase-coated nanoparticles loaded with ATO
Sav-D-VC NPs	Savinase-coated nanoparticles loaded with D-VC
Sav-NPs	Savinase-coated nanoparticles
SD	standard deviation
SEM	scanning electron microscopy
ULA	ultra-low attachment (cell-culture surface)

1 INTRODUCTION

1.1 KRAS mutations in colorectal cancer significantly complicate treatment due to resistance and uncontrolled cell proliferation

Colorectal cancer (CRC) is globally recognized as the third most commonly diagnosed cancer and the second leading cause of cancer mortality [1]. This makes it a major global concern. The treatment of CRC is particularly complicated by KRAS mutations, which are found in approximately 40% of CRC cases [2]. The KRAS protein, a small GTPase, plays a crucial role in regulating cell proliferation, differentiation, and survival signaling pathways. Mutations in KRAS result in uncontrolled proliferation and drug resistance, complicating treatment efforts and contributing to high mortality rates [3]. Although KRAS mutations historically posed a significant therapeutic challenge, recent advancements have introduced potential targeted therapies [4].

1.2 The combination of arsenic trioxide (ATO) and D-vitamin C (D-VC) targets KRAS-mutant CRC cells by inducing oxidative stress and is currently undergoing clinical trials

The combination of arsenic trioxide (ATO) and D-vitamin C (D-VC) is considered a promising targeted therapy for KRAS-mutant colorectal cancer, and it has entered Phase II clinical trials in 2024 (NCT05721872) This treatment relies on the synergistic activity of ATO and D-VC to induce oxidative stress and selectively kill KRAS-mutant cancer cells. ATO causes mitochondrial dysfunction and initiates apoptosis by increasing reactive oxygen species (ROS) levels. On the other hand, D-VC enhances this effect by reducing the amount of intracellular glutathione (GSH), which is a major antioxidant in cells, making them more vulnerable to oxidative damage. After entering the cell through GLUT1 transporters, D-VC is converted to dehydroascorbate (DHA), which further adds to the oxidative stress inside the cancer cell (Figure 1) [4, 5]. Also, the chirality of vitamin C is important, since D-VC has shown to be more effective than the natural L-form [6]. This dual action helps surpass the oxidative threshold that is needed to damage mitochondrial oxidative phosphorylation complexes, leading to the release of cytochrome c and activation of apoptosis, while not affecting healthy tissues [4]. Importantly, the combined mechanism has shown strong effectiveness in studies, including 2D cell cultures

and mouse xenograft models [7]. These findings highlight the potential of ATO/D-VC as a targeted therapy for overcoming drug resistance in KRAS-mutant CRC.

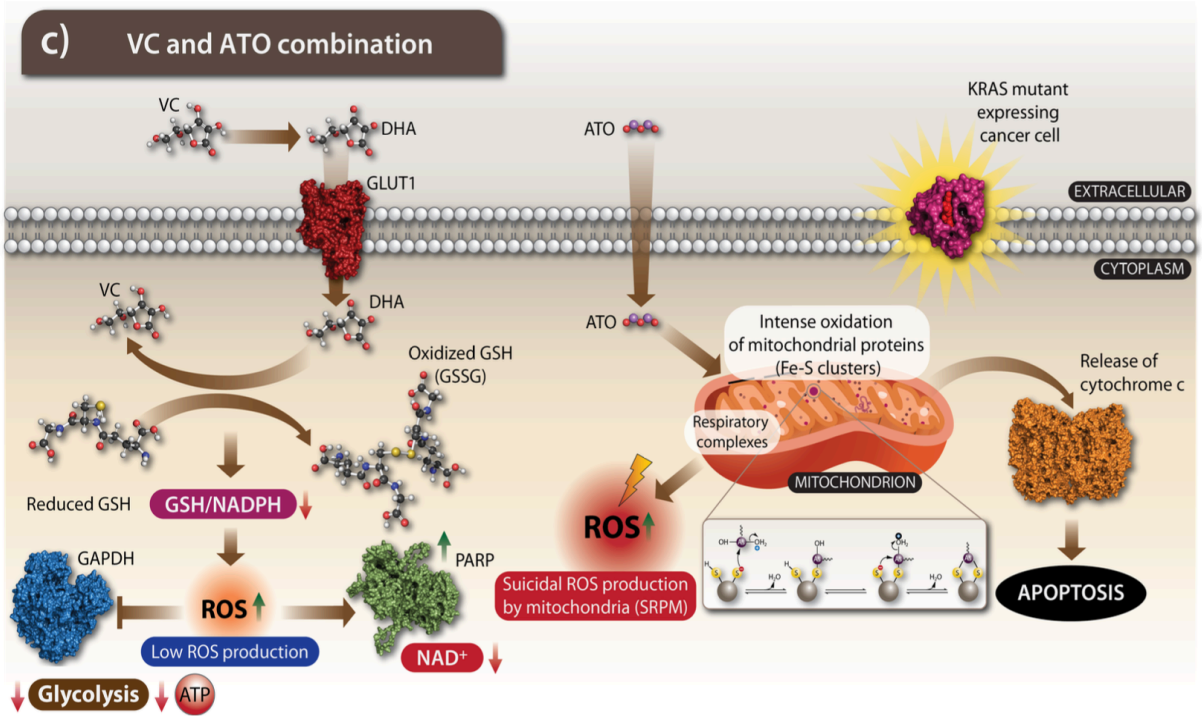

Figure 1. Schematic illustration of the synergistic cytotoxic mechanism of vitamin C (VC) and arsenic trioxide (ATO) co-treatment in KRAS-mutant cancer cells. The combination increases oxidative stress by depleting intracellular GSH and oxidizing mitochondrial proteins, leading to excessive ROS production and apoptosis. Reproduced from Burska et al. [4].

Despite these promising results, preclinical research was primarily conducted on 2D cell cultures or animal models, limiting insights into treatment efficacy within the complex tumor microenvironment. Thus, this study addresses an important gap by using a 3D CRC cell model called clusteroids for evaluating ATO/D-VC treatment.

1.3 Three-dimensional clusteroid models provide a more accurate simulation of tumor complexity and drug response than traditional 2D cell cultures

Three-dimensional (3D) cell cultures are *in vitro* models that have emerged as essential tools in cancer research due to their improved ability to replicate the structural and functional characteristics of solid tumors typically observed *in vivo*. Unlike traditional 2D monolayers, which do not capture spatial gradients of oxygen, nutrients, and signaling molecules, 3D models

allow for the formation of hypoxic cores and support more realistic cell–cell and cell–matrix interactions. These features are particularly important for evaluating drug responses and understanding resistance mechanisms in a tumor-like environment [8-10].

Clusteroids, a specific type of scaffold-free 3D model, are compact multicellular aggregates that mimic key aspects of tumor physiology. Their formation relies on the self-assembly of cells in a controlled microenvironment without the use of external scaffolds. A widely adopted method for generating clusteroids involves the use of a water-in-water (w/w) Pickering emulsion, which is based on an aqueous two-phase system (ATPS) consisting of dextran (DEX) and poly(ethylene oxide) (PEO). In this system, cells suspended in the DEX phase are encapsulated in droplets, while the continuous phase consists of PEO. This formulation allows cells to be confined in an aqueous microenvironment and promotes aggregation under gentle conditions [10-12]. To initiate clusteroid formation, osmotic compression is induced by adding a more concentrated PEO solution (typically increasing from 5.5% to 10–12% w/v), which draws water out of the DEX droplets. This dehydration step forces the cells into close proximity, enhancing cell–cell interactions and compacting them into nearly spherical clusteroids within hours. A schematic representation of the clusteroid formation process via ATPS emulsion is shown in Figure 2. Importantly, this method avoids the need for centrifugation or synthetic scaffolds, while preserving high cell viability [10,12].

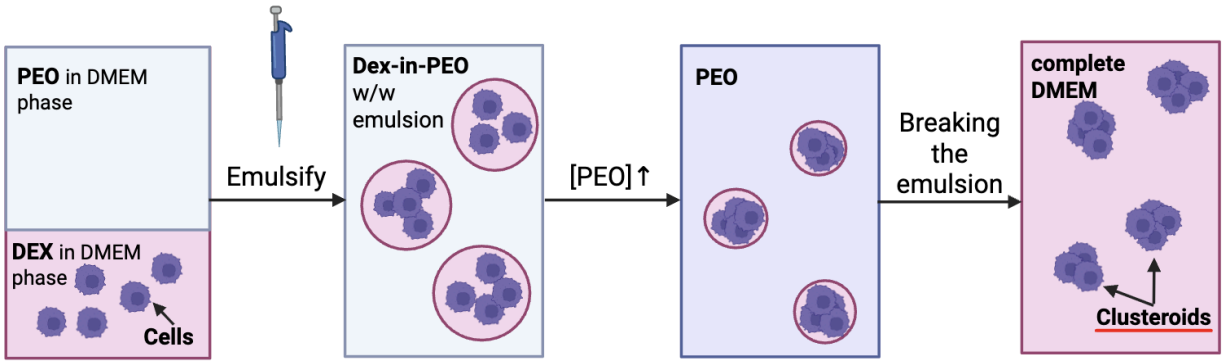

Figure 2. Schematic of clusteroid formation via ATPS-based Pickering emulsion. Cells suspended in the DEX-rich phase are emulsified into the PEO-rich continuous phase, forming DEX-in-PEO droplets. Upon increasing the PEO concentration, osmotic compression induces cell compaction within the droplets. Breaking the emulsion in by dilution with DMEM releases mature clusteroids. Created with BioRender.com.

The ATPS-based Pickering emulsion method offers a biocompatible and scalable strategy for generating 3D clusteroids with controlled size and high reproducibility [19-23]. Unlike traditional 3D culture techniques, this approach enables the efficient formation of dense and uniform spheroids, addressing limitations such as low yield and size variability. Its adaptability to coculture systems and relevance to tissue-like organization make it particularly useful for cancer modeling and preclinical drug screening. Recent applications, such as endothelial-hepatocyte clusteroids exhibiting spontaneous angiogenic sprouting and keratinocyte clusteroids used for evaluating antibacterial nanoparticle therapies, further demonstrate the platform's ability to simulate complex tissue microenvironments. An example of such an application is shown in Figure 3, where 3D clusteroids are used to evaluate the efficacy of nanoparticle-based drug delivery systems [10]. These examples highlight its utility in studying treatment responses that depend on multicellular interactions, drug penetration, and microenvironmental modulation [8–12].

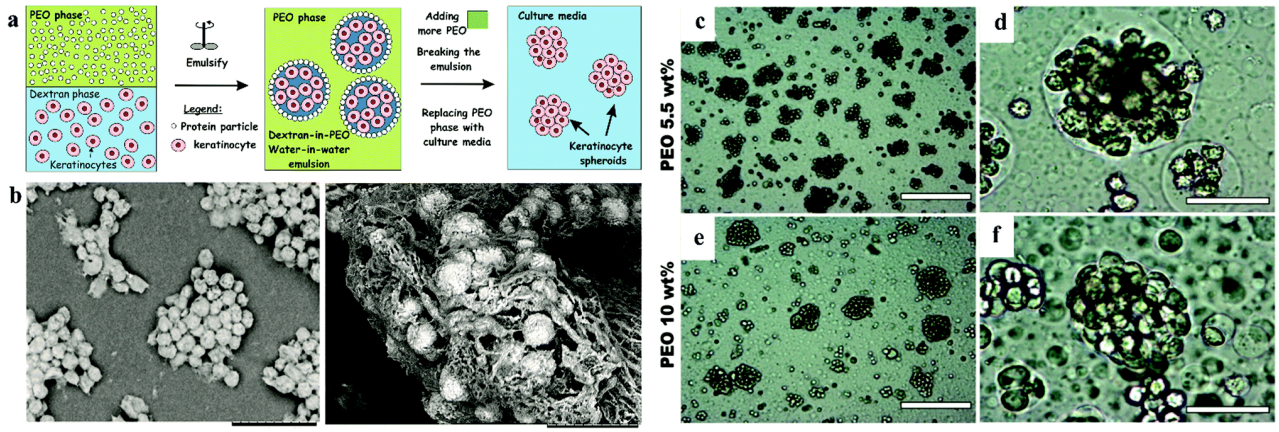

Figure 3. Formation of keratinocyte clusteroids using an ATPS-based Pickering emulsion. (a) Schematic showing keratinocytes in dextran-rich droplets stabilized by protein particles in a PEO-rich phase; osmotic dehydration induces clusteroid compaction. (b) SEM images of clusteroid aggregates. (c–f) Optical images showing the impact of increasing PEO concentration on spheroid density. Reproduced from Wang et al. [8].

Given the structural complexity and extracellular matrix (ECM) barriers present in 3D CRC cell models, the ATO/D-VC combination is expected to exhibit reduced cytotoxicity compared to 2D cultures. It is likely that the treatment primarily affects cells at the periphery of the clusteroids, with limited impact on cells deeper within the core.

1.4 Nanoparticle drug delivery systems significantly improve the therapeutic potential of drugs by enhancing permeability and controlled release

Encapsulating oxidative drugs in nanoparticles (NPs) offers major advantages in treating solid tumors, where dense extracellular matrix (ECM) often limits drug diffusion. NPs overcome these barriers due to their small size and tunable surface properties, which improve permeability and targeted delivery [13,14].

NPs can be composed of polymers, lipids, or metals, and optimized for efficient drug loading and release. A wide range of anticancer agents—including doxorubicin, paclitaxel, and gemcitabine—have been successfully encapsulated into NPs to improve pharmacokinetics, reduce systemic toxicity, and enhance tumor-specific drug accumulation [15]. For example, Zhu et al. [26] successfully fabricated a Prussian blue-based nanosystem (PB NPs as the photothermal drug nanocarrier) from using a hydrothermal method. The nanocarrier showed strong singlet oxygen-generated capacity upon IR laser irradiation and also demonstrated excellent biocompatibility. Hyperthermia generated from the photothermal conversion effect of HPB NPs also killed HepG2 cells in vitro, and enhanced tumor apoptosis under PDT.

Recently, Wang et al. [14] used 3D human hepatic tumour cell culture model to assess in-vitro the efficacy of "active" metformin-loaded nanoparticles (NPs) as anticancer therapeutics. The metformin nanocarrier design was repurposed from previous studies targeting bacterial and fungal biofilms with antimicrobials loaded in protease-coated nanoparticles [11, 16]. This approach has been used before in active nanocarriers of antibiotics to clear bacterial and fungal biofilms [24]. These active nanocarriers were constructed with shellac cores loaded with metformin as anticancer agent and featuring a surface coating of the cationic protease lysozyme. The lysozyme role as a nanocarrier surface coating is to partially digest the extracellular matrix (ECM) of the 3D tumour cell culture [18-23] which increases its porosity and the nanocarrier penetration. Hep-G2 hepatic 3D clusteroids were formed using a water-in-water (w/w) Pickering emulsion based on aqueous two-phase system (ATPS). Our specific metformin nano-formulation, comprising 0.2 wt% lysozyme-coated, 0.2 wt% metformin-loaded 0.2 wt% shellac NPs sterically stabilized by 0.25 wt% Poloxamer 407, demonstrated significantly enhanced anticancer efficiency on 3D hepatic tumour cell clusteroids. We examined the role of the lysozyme surface functionality of the metformin nanocarriers on their ability to kill both 2D and 3D hepatic tumour cell cultures. The anticancer efficiency at high metformin payloads was compared to this

at high concentration of nanocarriers at lower metformin payload. It was discovered that the high metformin payload NPs were more efficient than higher nanocarrier concentration at lower metformin payload. This study introduces a reliable in-vitro model for potential targeting of solid tumours with smart nano-therapeutics, presenting a viable alternative to animal testing for evaluating anticancer nanotechnologies.

Among these, polymeric NPs, such as those made from shellac, offer stability, biocompatibility, and controlled release. Shellac NPs are typically prepared by pH-induced co-precipitation: at alkaline pH (~10), shellac remains soluble and is mixed the water-soluble drug; then upon lowering the pH to 4–5.5, shellac precipitates and forms drug-loaded nanoparticles by intercalating the drug in their matrix. This method ensures high drug-loading efficiency, often exceeding 90% [14]. To improve colloidal stability and prevent aggregation, Poloxamer 407, a triblock copolymer surfactant, is used as a stabilizer. Poloxamer 407 also enhances biocompatibility and may prolong circulation time *in vivo* [14,16]. The schematic structure of these engineered drug-loaded nanoparticles, including the shellac core, poloxamer coating, and surface-bound proteases, is illustrated in Figure 4.

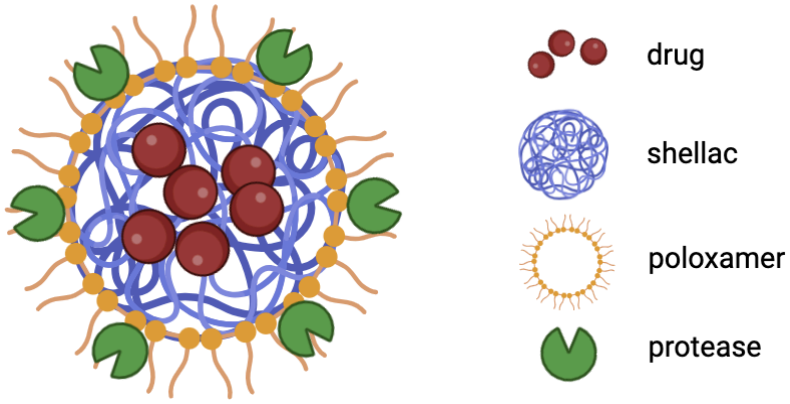

Figure 4. Schematic structure of protease-coated shellac–poloxamer nanoparticles. The nanoparticle core consists of drug molecules encapsulated in a shellac matrix, stabilized by a surface layer of poloxamer 407. Protease molecules are conjugated to the outer surface, enabling ECM degradation and improved cellular targeting through surface charge modulation. Created with BioRender.com.

Encapsulating oxidative drugs in shellac–poloxamer NPs protects them from premature degradation, allows sustained release, and increases the drug concentration reaching the tumor [13,15]. One key advantage of using such NPs is their ability to better penetrate the ECM,

especially when coated with proteases. These enzymes degrade ECM components (e.g., glycoproteins), increasing tissue porosity and enabling deeper NP penetration [14]. Moreover, proteases have high isoelectric points, imparting a positive surface charge to the NPs, which enhances interaction with negatively charged cancer cells or biofilms [14,16].

This dual functionality—ECM degradation and surface charge modulation—makes protease-coated shellac NPs a promising platform for targeted drug delivery. Lysozyme-functionalized NPs have shown enhanced anticancer efficacy in 3D tumor models and have also been repurposed for antifungal therapies due to their ability to disrupt biofilms [14,16].

In this study, we selected Savinase, a serine protease derived from *Bacillus* species, for the coating of the nanoparticles carrying oxidative drugs. Savinase is well-known for its strong proteolytic activity and stability across a broad pH range [17], making it a suitable candidate for enhancing NPs penetration through ECM-rich tumor environments.

Protease-coated shellac NPs have demonstrated significant improvements in therapeutic outcomes. For example, lysozyme-coated, metformin-loaded shellac NPs achieved over 90% reduction in tumor viability in 3D hepatic models—outperforming both free drugs and non-coated NPs [14]. These findings highlight the potential of protease-functionalized nanocarriers to enhance the intratumoral delivery of oxidative drugs and improve treatment efficacy in solid tumors and biofilm-associated infections [14,16].

Encapsulating ATO/D-VC in protease-coated nanoparticles is anticipated to improve its therapeutic efficacy in 3D CRC cell models by enhancing drug penetration and distribution, compared to the non-encapsulated formulation.

1.5 Significance of the Study

This study focuses on evaluating the effectiveness of ATO/D-VC in 3D colorectal cancer (CRC) models and exploring strategies to enhance its therapeutic potential through nanoparticle-mediated delivery and protease surface functionalization. To address this, the research involves the development and optimization of 3D clusteroid cultures derived from KRAS-mutant CRC cell lines, as well as a comparative analysis of the cytotoxic effects of ATO, D-VC, and their combination in both 2D and 3D cell models. In addition, the study includes the formulation of protease-coated shellac–poloxamer nanoparticles containing ATO and D-VC,

followed by the evaluation of their impact on cell viability and proliferation within 3D CRC clusteroids.

This study presents a targeted strategy to overcome key limitations in colorectal cancer therapy by combining oxidative drug treatment with a protease-functionalized nanoparticle-based delivery system. By improving drug penetration through the ECM of the 3D tumor cell culture and surface charge enhanced nanocarrrier accumulation, this approach aims to increase the therapeutic efficacy of ATO/D-VC and similar drugs in solid tumors while minimizing off-target effects.

Beyond KRAS-mutant CRC, this strategy offers broader potential for improving drug delivery in other hard-to-treat cancers and contributes to the advancement of 3D tumor modeling in preclinical research. Its application may support the development of more effective, less toxic cancer therapies and promote the adoption of personalized nanomedicine.

2 MATERIALS AND METHODS

2.1 Reagents

Table 1. Reagents for cell culturing

Reagent	**Brand**	**Catalog #**
DMEM (Dulbecco's Modified Eagle Medium), high glucose	Gibco	11965092
DMEM/F-12 (mixture of DMEM and Ham's F‑12 medium)	Gibco	11320033
Fetal Bovine Serum (FBS)	Gibco	A5256701
Penicillin-streptomycin solution	VWR Chemicals	392-0406
Dulbecco's phosphate-buffered saline (PBS) (10x)	Capricorn scientific	PBS-10XA
Trypsin-EDTA (0.05%)	Capricorn scientific	TRY-1B
Cellstripper	Corning	25056CI

Table 2. Reagents for creating clusteroids.

Reagent	Brand	Catalog #
Poly(ethylene oxide) average Mv 200,000 (nominal), powder	Sigma-Aldrich	181994
Dextran, MW ca 250,000	Thermofisher	J60200.36
DMEM/F-12	Gibco	11320033

Table 3. Reagents for nanoparticle formulation.

Reagent	Brand	Catalog #
Protease from Bacillus sp.	Sigma-Aldrich	P5985-50ML
SSB® AQUAGOLD	SSB	9000-59-3

Poloxamer 407	Sigma-Aldrich	16758

Table 4. Reagents for viability and cell proliferation evaluation.

Reagent	**Brand**	**Catalog #**
CellTiter 96® AQ_{ueous} One Solution Reagent	Promega	G3580
Hoechst 33342	Thermofisher	H1399
Propidium Iodide	Thermofisher	P1304MP
DMEM/F-12, no Phenol Red	Gibco	21041025

2.2 Cell cultures

Two human colorectal cancer cell lines with KRAS mutations were used in this study: HCT-116 (KRAS G13D mutation) and SW620 (KRAS G13V mutation). HCT116 cells were derived from a primary colon carcinoma, while SW620 cells were derived from a metastatic site in a lymph node. Cells were cultured in Dulbecco's Modified Eagle Medium (DMEM, Gibco) supplemented with 10% fetal bovine serum (FBS, Gibco) and 1% penicillin-streptomycin (10,000 U/mL, Thermo Fisher Scientific) under standard conditions (37 °C, 5% CO_2).

2.3 2D cell cultures seeding for ATO/D-VC treatment

HCT-116 and SW620 colorectal cancer cell lines were seeded into 6-well tissue culture-treated plates at densities of 200,000 and 600,000 cells per well, respectively, in 2 mL of DMEM/F12 (mixture of DMEM and Ham's F‑12 medium) supplemented with 10% FBS. The cells were incubated under standard conditions (37 °C, 5% CO_2) for 48 hours prior to treatment (see Figure 5 for workflow).

2.4 Generation of 3D cell models via clusteroid formation for ATO/D-VC treatment

2.4.1 Preparation of DEX-in-PEO pickering emulsion components

The clusteroid generation protocol was based on the principle of DEX-in-PEO Pickering emulsions as described by Wang et al. [8], while the specific experimental conditions—including polymer concentrations, incubation times, and emulsification technique—were developed and

optimized in this study. A 30 wt% stock solution of poly(ethylene oxide) (PEO, 200 kDa; Sigma-Aldrich) was prepared in Dulbecco's phosphate-buffered saline (PBS), allowed to hydrate for 24 hours at room temperature, sterilized by autoclaving, and centrifuged at 7800 rpm for 5 hours to remove silica particles commonly present in commercial PEO batches as an anticlumping agent. The resulting PEO stock solution was subsequently diluted to 15 wt% and 7.5 wt% using DMEM/F12 supplemented with 20% fetal bovine serum (FBS). In parallel, a 7.5 wt% dextran (DEX, 450 kDa; Sigma-Aldrich) solution was prepared in DMEM containing 10% FBS and sterilized by passing through a 0.22 μm syringe filter.

2.4.2 Preparation of clusteroids for ATO/D-VC treatment

For making 3D cell culture, trypsinized HCT116 or SW620 cells were collected and transferred to 5 mL Eppendorf tubes (200,000 and 600,000 cells per tube, respectively), centrifuged, and the resulting pellets were re-suspended in 20 μL of the 7.5 wt% DEX solution. Next, 80 μL of the 7.5 wt% PEO solution was layered over the DEX phase. A single-channel pipette (20-200 μL) was used to mix the solutions and form a DEX-in-PEO Pickering emulsion by pumping the mixture twice. An additional 900 μL of 15 wt% PEO was then added to the bottom of the tubes, allowing the clusteroids to settle naturally over 24 hours. To increase the external PEO concentration and promote clusteroid formation, 3mL of 15 wt% PEO solution was added to the bottom of each tube, and samples were incubated undisturbed for 24 hours at 37 °C. The clusteroids were then collected by centrifugation (5 min, 1000 rpm), and 200 μL of the pellet was transferred into ultra-low attachment 24-well plates. To break the DEX-in-PEO emulsion and release the cell clusteroids, 2 mL of DMEM/F12 supplemented with 10% FBS was added to each well. The clusteroids were then incubated for 24 hours at 37 °C to allow recovery and maturation in standard culture conditions prior to treatment (Figure 5 illustrates the timeline and setup).

2.5 ATO/D-VC treatment of 2D and 3D cell cultures

For both 2D and 3D cell cultures, the treatment with the oxidative drug combination (ATO and D-VC) was performed by replacing the existing culture medium with fresh DMEM/F12 supplemented with 10% FBS. Cells were then treated with 7.5 μM ATO, 1.5 mM D-VC and their combination. Working solutions of both drugs were kindly provided by Dr.

Sarbassov's laboratory team. Treatments were performed in parallel for both culture systems to ensure consistency in experimental conditions (Figure 5).

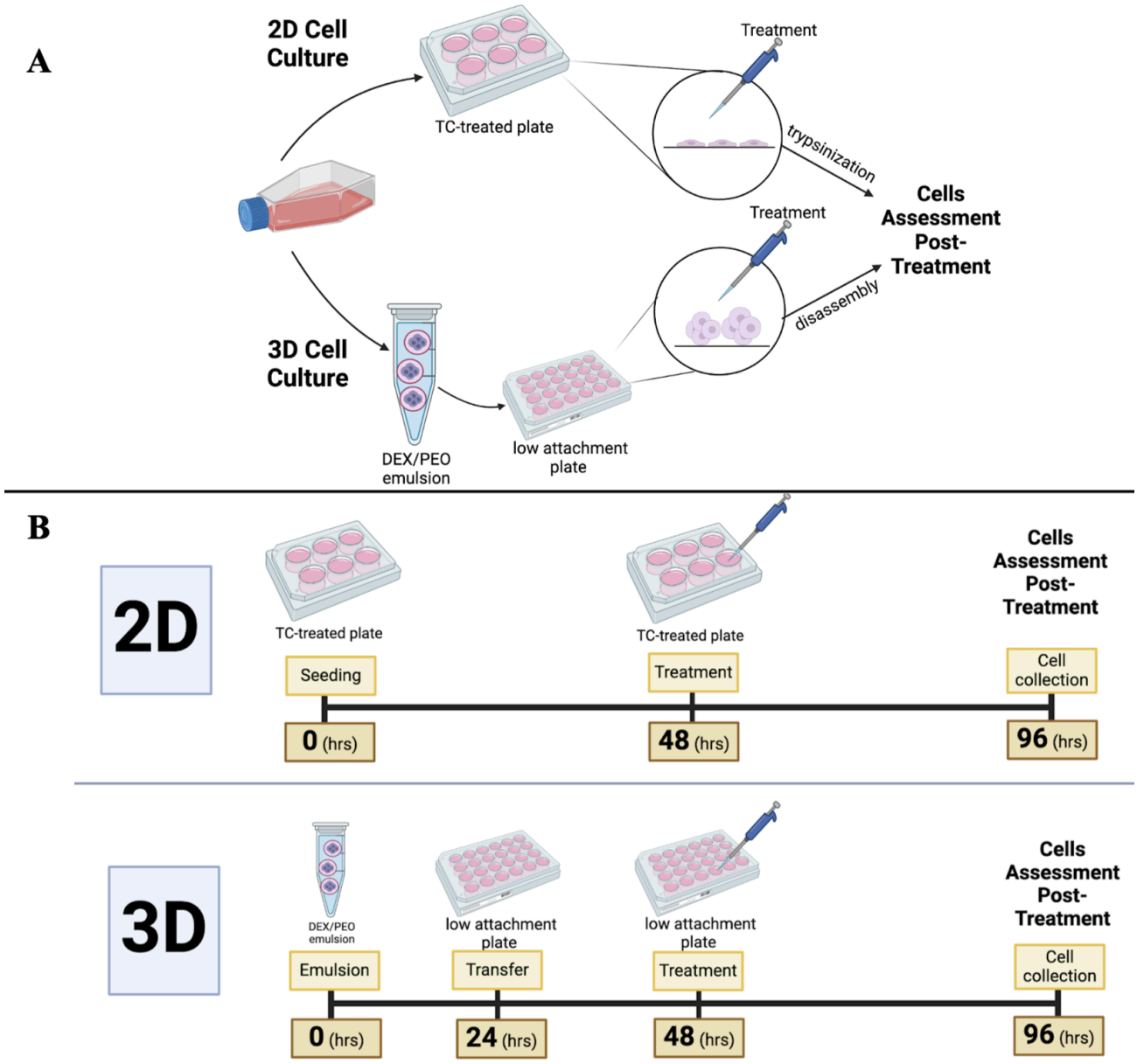

Figure 5. Workflow for 2D and 3D colorectal cancer cell cultures treated with ATO/D-VC. (a) Schematic of 2D and 3D culture preparation, drug treatment, and post-treatment assessment. 3D clusteroids were formed using DEX/PEO emulsions and cultured in ultra-low attachment plates; (b) Timeline of experimental steps. In 2D cultures, cells were seeded (0 h), treated (48 h), and collected (96 h). In 3D cultures, clusteroids were formed (0 h), transferred (24 h), treated (48 h), and collected (96 h). Created with Biorender.com.

2.5 Preparation of working solutions for nanoparticle formulation

2.5.1 Shellac solution

A 0.6 wt% shellac solution was prepared by diluting the commercial 25 wt% shellac stock solution (SSB® AQUAGOLD, CAS No. 9000-59-3) in Milli-Q water under constant stirring until fully dissolved. The solution was stored at 4 °C and used within 48 hours.

2.5.2 Poloxamer 407 solution

Poloxamer 407 (Sigma-Aldrich) powder was dissolved in Milli-Q water to a final concentration of 0.3 wt%. The solution was stirred until fully dissolved and stored at 4 °C.

2.5.3 Savinase solution

A 0.6 wt% Savinase stock solution was prepared by diluting 0.6 mL of liquid Savinase® 16L into Milli-Q water to a final volume of 100 mL. The solution was sonicated in an ultrasonic bath for 15 min to minimize enzyme aggregation before use.

2.6 Formulation of shellac–poloxamer nanoparticles

Shellac–poloxamer nanoparticles were formulated using a pH-driven precipitation method. All formulations had a final volume of 4.5 mL, with adjustments in Milli-Q water volume made to accommodate drug loading while maintaining constant polymer concentrations.

2.6.1 Unloaded nanoparticles

To prepare unloaded nanoparticles (i.e., without ATO or D-VC), 1 mL of 0.3 wt% poloxamer 407, 1 mL of 0.6 wt% shellac, and 2.5 mL of Milli-Q water were mixed (final concentrations: 0.067 wt% poloxamer 407, 0.133 wt% shellac). The pH was increased to 10 using 0.25 M NaOH and sonicated using a probe sonicator at 35% amplitude (15 s on, 15 s off) for a total of 1 min 15 s. The pH was then lowered to 2.5–2.75 with 0.25 M HCl. If visible aggregates formed, the dispersion was sonicated again at 20% amplitude for 1 min. Finally, the pH was increased to 5 to avoid over-aggregation. The formulation was sterilized by filtration through a 0.22 µm syringe filter.

2.6.2 ATO-loaded nanoparticles

For ATO-loaded NPs, 1 mL of 0.3 wt% poloxamer, 1 mL of 0.6 wt% shellac, and 2.054 mL of Milli-Q water were combined. After pH elevation and sonication, the pH was

adjusted to 7.0. Then, 446 µL of 50.5 mM ATO solution was added. The pH was decreased to 2.5–2.75 and finally adjusted to 5 before filtration.

2.6.3 D-VC-loaded nanoparticles

To prepare D-VC-loaded NPs, 1 mL of 0.3 wt% poloxamer 407, 1 mL of 0.6 wt% shellac, and 1.885 mL of Milli-Q water were used. After sonication and pH adjustment to 7.0, 615 µL of 732 mM D-VC solution was added. The pH was lowered to 2.5–2.75 and then adjusted to 5. The formulation was filtered as described above.

2.7 Coating with Savinase

2.7.1 Optimization of conditions for NPs coating with Savinase

To determine the optimal pH for Savinase coating, the zeta potential of both uncoated nanoparticles and free Savinase was measured at pH 3 to 7. Unloaded nanoparticles were prepared, centrifuged, and resuspended in Milli-Q water adjusted to the target pH. Free Savinase solutions (0.6 wt%) were prepared by aliquoting a working stock and individually adjusting the pH of each aliquot using 0.25 M HCl or NaOH. Each aliquot of unloaded nanoparticles and Savinase solution was then measured for zeta potential at 25 °C using DLS measurements (Litesizer 500 , Anton Paar, Austria). Results were plotted in Microsoft Excel to identify the pH where NPs were maximally negative and Savinase maximally positive. This pH, corresponding to the greatest electrostatic attraction, was used for all subsequent Savinase coating steps.

2.7.2 Optimization of concentration for NPs coating with Savinase

To determine the most effective Savinase concentration for coating without inducing aggregation or over-saturation, Savinase solutions ranging from 0 to 0.6 wt% were prepared. Pellets of unloaded nanoparticles were resuspended in 1 mL of each concentration at pH 5, selected based on zeta potential analysis described in Section 2.7.1, incubated for 30 min, and centrifuged at 14,500 rpm for 15 min. Pellets were then washed and resuspended in Milli-Q water. Hydrodynamic diameter and zeta potential were measured via dynamic light scattering (DLS). The optimal concentration was selected based on achieving a positive surface charge without evidence of aggregation.

2.7.3 Coating of nanoparticles with Savinase

Unloaded, ATO-loaded, and D-VC-loaded nanoparticles were coated using the Savinase concentration and pH conditions optimized in Sections 2.7.1 and 2.7.2 (0.6 wt%, pH 5,

respectively). For coating, NP suspensions (1 mL) were centrifuged at 14,500 rpm for 15 minutes, the supernatants discarded, and the pellets resuspended in 1 mL of Savinase solution prepared at the optimized pH. After 30 minutes of gentle shaking, the samples were centrifuged again and resuspended in 1 mL of DMEM/F12 medium supplemented with 10% FBS for downstream use.

To confirm successful coating and validate the nanoparticle size measured by DLS, the prepared Savinase-coated nanoparticles were visualized by scanning electron microscopy (SEM). Additionally, to assess their interaction with 3D cell structures, HCT116 clusteroids were incubated with unloaded Savinase-coated nanoparticles for 4 hours, fixed, and imaged using SEM to observe nanoparticle accumulation on the cell surface.

2.8 Nanoparticle dosing for 3D cell treatment

For the treatment of 3D cell cultures, Savinase-coated ATO- or D-VC-loaded nanoparticles were added to wells containing pre-formed clusteroids in ultra-low attachment plates. Prior to treatment, the medium in each well was refreshed with DMEM/F12 supplemented with 10% FBS. A total of 30 µL of nanoparticle suspension was then added per condition. The final volume in each well was adjusted to 2 mL using additional DMEM/F12 + 10% FBS, resulting in final drug concentrations of 7.5 µM ATO and 1.5 mM D-VC. These concentrations were calculated based on the assumption of complete (100%) encapsulation efficiency to standardize dosing across all experimental groups and were selected to match the concentrations used for treatment with the free drug formulations.

2.9 Collection of cells for assessment of treatment effectiveness

Following 48 hours of treatment, cells were harvested for downstream viability and proliferation assays. Cell collection procedures were optimized to ensure minimal stress and consistent handling across formats.

2.9.1 Collection of cells from 2D culture

For 2D cultures, the medium containing floating cells was first collected from each well into a 15 mL tube. Wells were then rinsed with phosphate-buffered saline (PBS) to remove serum residues and prepare the surface for further trypsinization. The rinse was added to the same tube. The cell suspension was centrifuged at 400 × g for 5 min, and the supernatant was discarded.

Meanwhile, adherent cells were detached using 0.05% Trypsin-EDTA. Trypsinization was neutralized by adding an equal volume of DMEM/F12 without Phenol Red but supplemented with 10% FBS. The trypsinized cells were transferred to the same tube containing the previously centrifuged pellet, and the combined cell pellet was gently resuspended in fresh DMEM/F12 (no Phenol Red, +10% FBS) for further analysis.

2.9.2 Collection of cells from 3D culture

For 3D clusteroid cultures, the clusteroids were first collected from ultra-low attachment wells and transferred to centrifuge tubes. The suspension was centrifuged at 400 × g for 5 min, and the supernatant was aspirated. The pellet was resuspended in PBS to wash residual serum and media, then centrifuged again under the same conditions. After removing the supernatant, the clusteroids were resuspended in Cellstripper™ (Corning) and incubated for 15-20 minutes to enzymatically dissociate the 3D structure. The reaction was neutralized using DMEM/F12 without Phenol Red supplemented with 10% FBS. The resulting single-cell suspension was used for viability and proliferation measurements.

2.10 Treatment effectiveness assessment assays

To evaluate the therapeutic efficacy of ATO, D-VC and their combination in different formulations, cell viability, cell proliferation, and morphological analysis assays were performed on the treated 2D and 3D cell cultures. Collected HCT116 and SW620 cells (section 2.9) from the untreated control group were seeded at 15,000 and 70,000 cells per well, respectively, in tissue culture-treated 96-well plates (Corning). The same volumes of single-cell suspensions were used for all treated conditions to ensure consistency across experimental groups. MTS absorbance values were evaluated as percentage relative to the untreated control to quantify the impact of the applied treatment on the cell proliferation.

2.10.1 Cell proliferation assessment using MTS assay

Proliferation rates were quantified using the CellTiter 96® AQueous One Solution Cell Proliferation Assay (MTS, Promega). Equal volumes of treated and control cell suspensions were seeded into tissue culture-treated 96-well plates, followed by the addition of MTS reagent according to the manufacturer's protocol. The MTS assay is based on the bioreduction of the MTS tetrazolium compound by metabolically active (viable) cells into a soluble formazan product. This reaction is mediated by NAD(P)H-dependent dehydrogenase enzymes and

produces a colored byproduct in the culture medium [27]. After 1.5 hour of incubation at 37 °C, absorbance at 490 nm was measured using a FLUOstar Omega Microplate Reader. The percentage of proliferation was calculated relative to untreated controls and processed in Microsoft Excel.

2.10.2 Viability assessment using Hoechst/Propidium Iodide (PI) staining

Cell viability was assessed using dual fluorescent staining with Hoechst 33342 and Propidium Iodide (PI). After treatment and collection (Section 2.9), equal volumes of each cell suspension were seeded into tissue culture-treated 96-well plates. Cells were incubated with 2 µM PI and 0.2 µM Hoechst 33342 for 45 minutes at 37 °C, protected from light. Fluorescent images were captured using an Olympus CKX53 inverted microscope equipped with a U-RFL-T mercury burner. Hoechst 33342 permeates all cell membranes and binds to DNA, staining the nuclei of both live and dead cells, while PI is membrane-impermeable and only enters cells with compromised membranes, making it selective for non-viable cells.

Image analysis was conducted using ImageJ software to quantify the number of total and PI-positive (dead) cells. The percentage of viable cells was calculated in Microsoft Excel using the following formula:

$$\%\ viable\ cells\ =\ (1\ -\ \frac{number\ of\ dead\ cells}{number\ of\ total\ cells})\times 100\%$$

2.10.3 Morphological assessment of 3D clusteroid growth

To assess drug-induced morphological changes in 3D cell models, brightfield microscopy was performed to monitor clusteroid growth at various time points. Images of clusteroids were acquired before and after treatment using the Olympus CKX53 microscope. The width of individual clusteroids was measured using ImageJ by manually tracing and analyzing each clusteroid from the acquired images. The resulting measurements were visualized using box plots in RStudio. This analysis enabled comparison of size distribution between the untreated control and treated clusteroids, providing an additional morphological indicator of therapeutic efficacy.

2.11 Statistical Analysis

To evaluate statistical differences between treatment groups, two-sample unpaired, two-tailed Student's *t*-tests were conducted. Prior to each comparison, Levene's test was used to

assess the assumption of equality of variances. In instances where variances were found to be unequal ($p < 0.05$), a Welch's *t*-test would have been applied; however, equal variances were confirmed in all cases ($p > 0.05$), and standard *t*-tests were used throughout.

When multiple treatment groups were compared to a single reference group (e.g., control), Bonferroni correction was applied to account for multiple comparisons and to ensure the reliability of significance levels. Corrected *p*-values were interpreted as significant when $p < 0.05$, very significant when $p < 0.01$, and highly significant when $p < 0.001$. For direct pairwise comparisons between 2D and 3D culture conditions, no correction for multiple comparisons was applied, as each comparison was predefined and tested only once.

Statistical significance was indicated directly in the corresponding figures using standard asterisk notation.

3 AIMS OF THE THESIS PROJECT

The **first hypothesis** for the current research is that the oxidative drug combination of arsenic trioxide (ATO) and D-vitamin C (D-VC) exhibits reduced efficacy in 3D colorectal cancer (CRC) models compared to its action on 2D cultures, due to limited penetration of the drugs through the extracellular matrix (ECM). It is anticipated that ATO/D-VC will primarily affect the peripheral cells in 3D clusteroids, with reduced impact on cells within the core.

To address this hypothesis, the following research aim has been defined:

Aim 1. Compare the efficacy of the ATO/D-VC treatment in 2D and 3D colorectal cancer cell models

Objectives:

- To develop and optimize 3D clusteroid cultures from KRAS-mutant CRC cell lines.
- To evaluate the cytotoxic and antiproliferative effects of ATO, D-VC, and their combination in 2D and 3D cell models.
- To assess the differences in the cell viability and proliferation between the two culture systems.

A **second hypothesis** is that nanoparticle-mediated delivery of ATO/D-VC using protease-functionalized nanocarriers enhances the treatment effectiveness in 3D CRC models by improving ECM penetration in the cell clusteroids and the drug accessibility to inner cell layers.

To address this hypothesis, the following research aim has been defined:

Aim 2. Evaluate the effectiveness of protease-coated nanoparticle-mediated delivery of ATO/D-VC in 3D colorectal cancer models.

Objectives:

- To formulate and characterize protease-coated shellac–poloxamer nanoparticles loaded with ATO and D-VC.
- To treat 3D clusteroids with the active nanoparticle formulations and assess cell viability and proliferation.
- To compare the therapeutic effect of nanoparticle-mediated delivery with that of the free drugs.

4. RESULTS

4.1 Evaluation of ATO/D-VC combination in 2D monolayer cultures

To investigate the cytotoxic effects of the oxidative drug combination ATO/D-VC in 2D models, HCT116 and SW620 CRC cells were treated with ATO (7.5 μM), D-VC (1.5 mM), or their combination for 48 hours. Representative brightfield images (Figure 6A–D, Figure 7A–D) revealed visible morphological changes, including reduced confluency, cell rounding, detachment, and shrinkage, which were most pronounced in the combination treatment group. MTS assay results (Figures 6E and 7E) showed that ATO/D-VC treatment reduced cell proliferation to approximately 60% of control levels in HCT116 cells and to about 40% in SW620 cells. This corresponds to a reduction of roughly 1.7-fold and 2.5-fold, respectively, when compared to untreated controls. In both cell lines, the effect of the combination was at least twofold greater than that observed for either single agent, indicating a significant enhancement in antiproliferative activity. This trend was further supported by Hoechst/PI viability assay results (Figures 6F and 7F), where ATO/D-VC reduced viability to under 30% in HCT116 and to below 25% in SW620 cells—representing more than a three-fold decrease compared to untreated controls. Interestingly, the combination was especially effective in SW620 cells, which showed only mild reductions in viability with ATO or D-VC alone. Overall, quantitative analysis of the results from the MTS and Hoechst/PI assays demonstrated that the combination of ATO and D-VC significantly reduced both cell proliferation and viability in comparison to single-agent treatments or untreated control, indicating a synergistic cytotoxic effect.

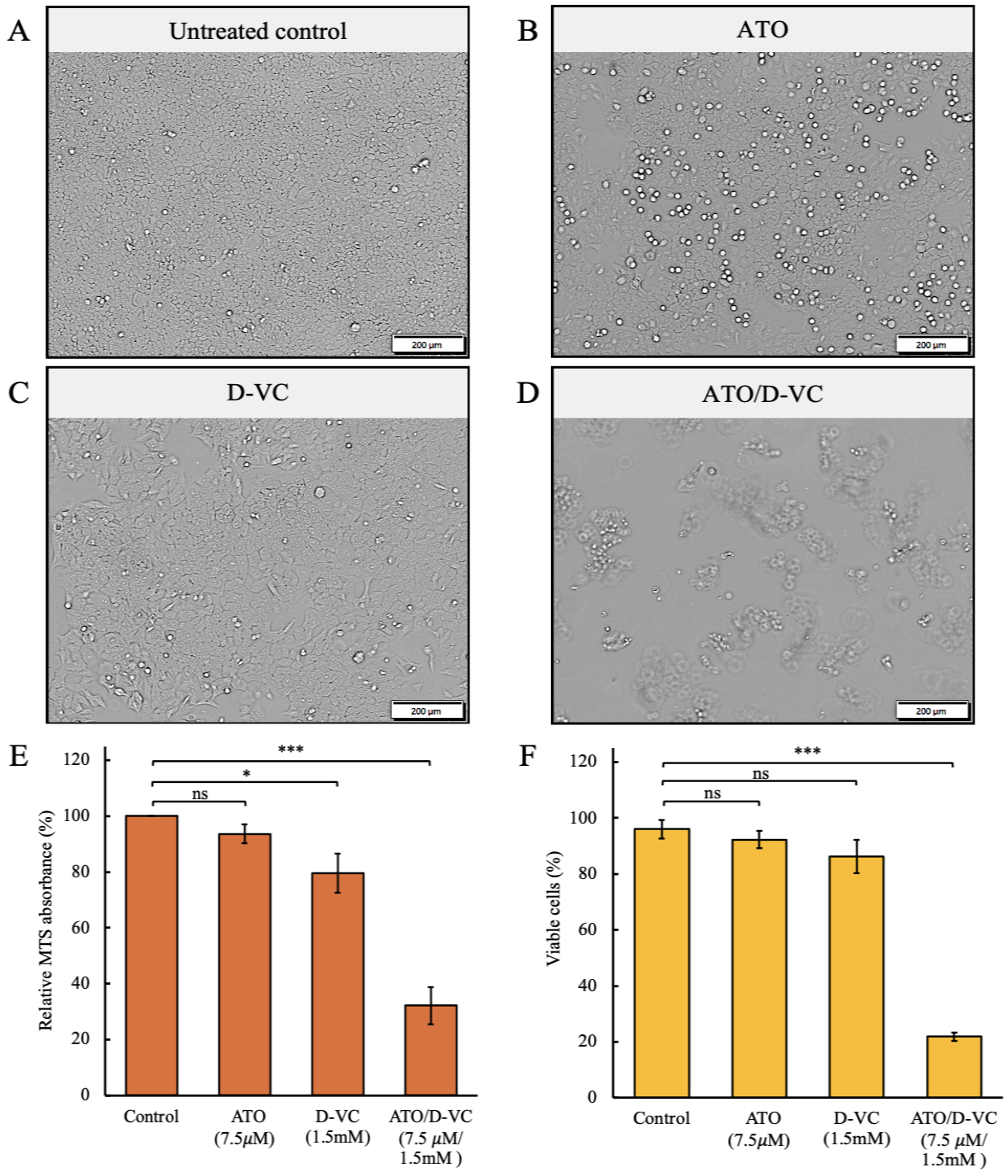

Figure 6. Effect of oxidative drug combinations on HCT116 cells in 2D culture. (A–D) Representative brightfield images of HCT116 cells after 48-hour treatment under 2D culture conditions: (A) Untreated control; (B) ATO (7.5 µM); (C) D-VC (1.5 mM); (D) ATO/D-VC combination (7.5 µM / 1.5 mM). Scale bars: 200 µm. **(E)** Cell proliferation measured by MTS assay. **(F)** Cell viability assessed via Hoechst/PI assay. Data represent mean ± SD from three independent biological replicates performed in technical triplicates. Statistical comparisons were performed using unpaired, two-tailed Student's t-tests with Bonferroni correction. Statistical significance is indicated as follows: ns = not significant; *p < 0.05; ***p < 0.001.

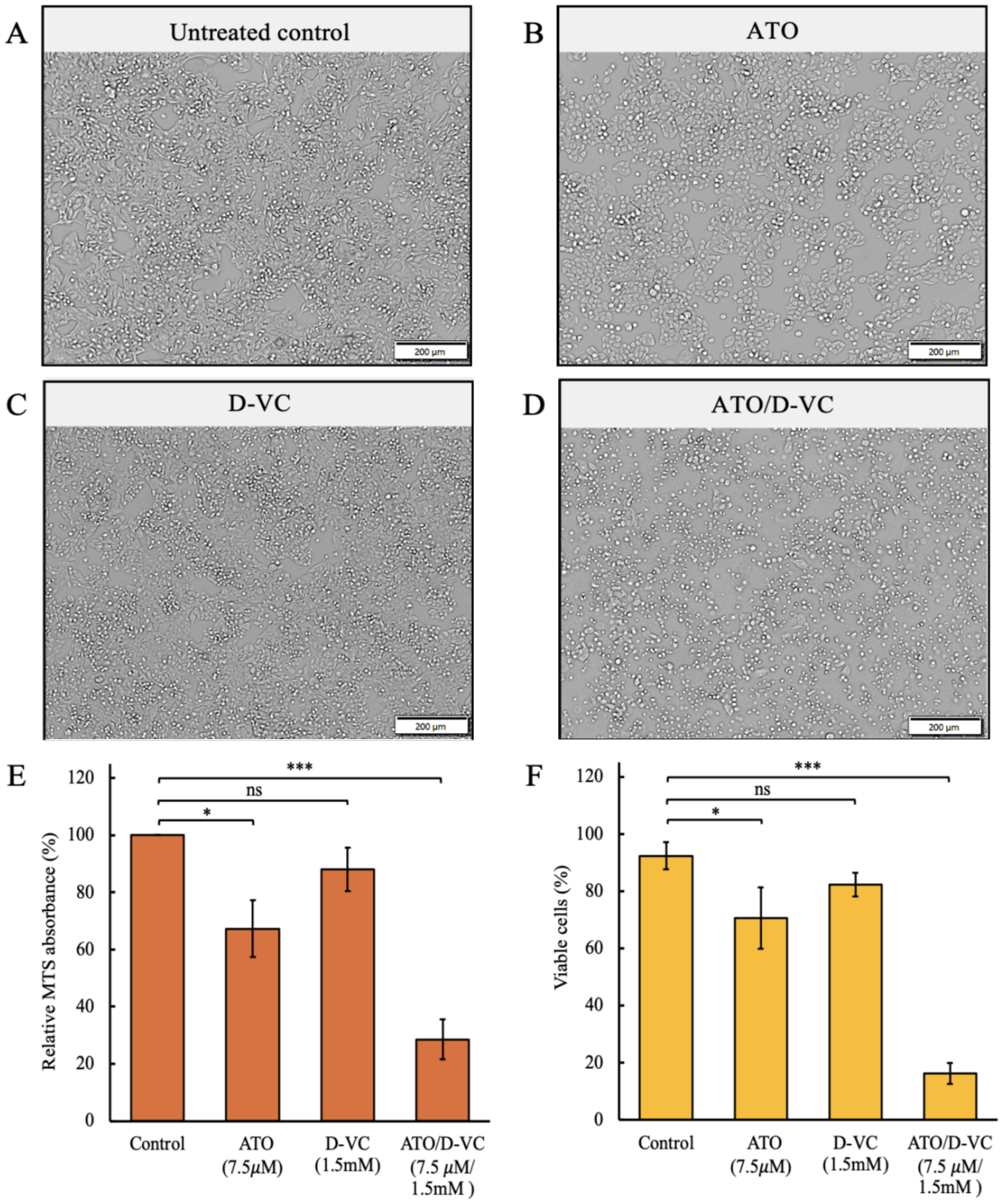

Figure 7. Effect of oxidative drug combinations on SW620 cells in 2D culture. (A–D) Representative brightfield images of SW620 cells after 48-hour treatment under 2D culture conditions: (A) Untreated control; (B) ATO (7.5 µM); (C) D-VC (1.5 mM); (D) ATO/D-VC combination (7.5 µM / 1.5 mM). Scale bars: 200 µm. **(E)** Cell proliferation measured by MTS assay. **(F)** Cell viability assessed via Hoechst/PI assay. Data represent mean ± SD from three independent biological replicates performed in technical triplicates. Statistical comparisons were performed using unpaired, two-tailed Student's t-tests with Bonferroni correction. Statistical significance is indicated as follows: ns = not significant; *$p < 0.05$; ***$p < 0.001$.

4.2 Formation and growth assessment of 3D clusteroids

To establish 3D clusteroid models with optimal size (preferably above 100 μm), different emulsification strategies for DEX-in-PEO ATPS emulsion were explored. Initially, the syringe-based method described by Wang et al. [8] was applied, but the resulting clusteroids were too small and surrounded by a high number of unincorporated single cells. Therefore, we adopted a pipette-based emulsification approach, which led to the formation of larger, more compact clusteroids with significantly fewer residual single cells. These differences became especially evident after emulsion breakage and subsequent 24-hour incubation in DMEM supplemented with 10% FBS (Figure 8).

Next, we evaluated the effect of the well plate surface on the clusteroid maintenance and growth. Clusteroids seeded into standard tissue culture (TC)-treated plates began to adhere, spread and lose their 3D integrity over time (Figure 1S).

In contrast, when seeded into ultra-low attachment (ULA) plates, clusteroids retained their spherical morphology and grew in size while maintaining compactness and structural coherence. Brightfield images captured at 48 and 96 hours post-ATPS emulsion breakage illustrates this contrast in structural preservation (Figure A1).

Following optimization of emulsification and culture conditions, the growth of clusteroids was monitored over a 6-day period. Representative images revealed a gradual and consistent increase in size and density for both HCT116 and SW620 clusteroids (Figure 9A). Quantitative analysis confirmed a significant increase in clusteroid size from Day 2 to Day 6 for both cell lines (Figure 9B–C), supporting active proliferation and structural maturation. To standardize treatment response experiments, clusteroid sizes were measured after 48 hours of culture (pre-treatment), and analysis demonstrated uniform size distribution across all experimental groups (Figure A2 A–B), ensuring comparability in subsequent drug testing.

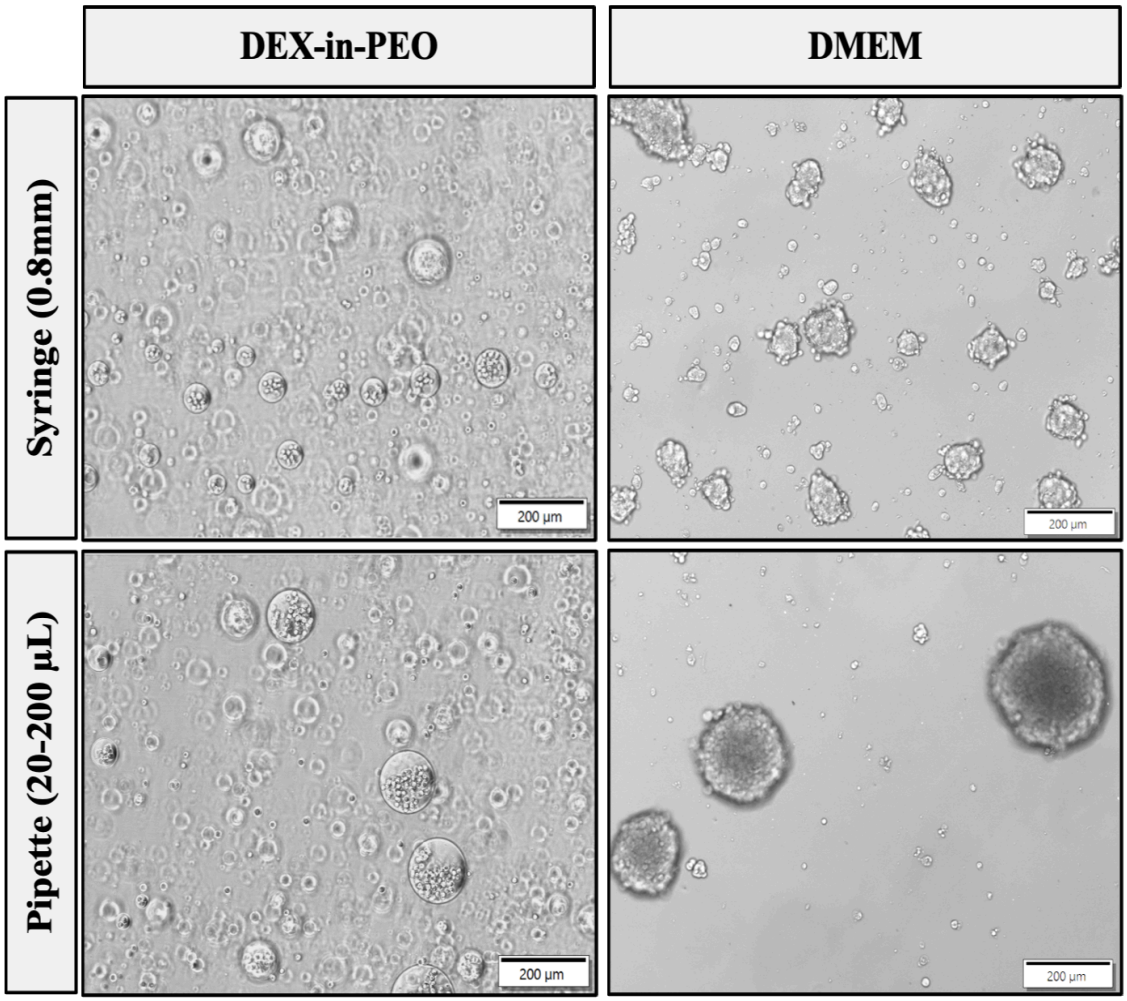

Figure 8. Formation of 3D SW620 clusteroids using different emulsification tools. Top row: clusteroids generated using a syringe with a 0.8 mm needle; Bottom row: clusteroids generated using a 20–200 µL pipette. Left column: clusteroids in DEX-in-PEO emulsion after 24-hour incubation; Right column: the same clusteroids imaged after 24-hour incubation in DMEM following emulsion breakage. Scale bars: 200 µm.

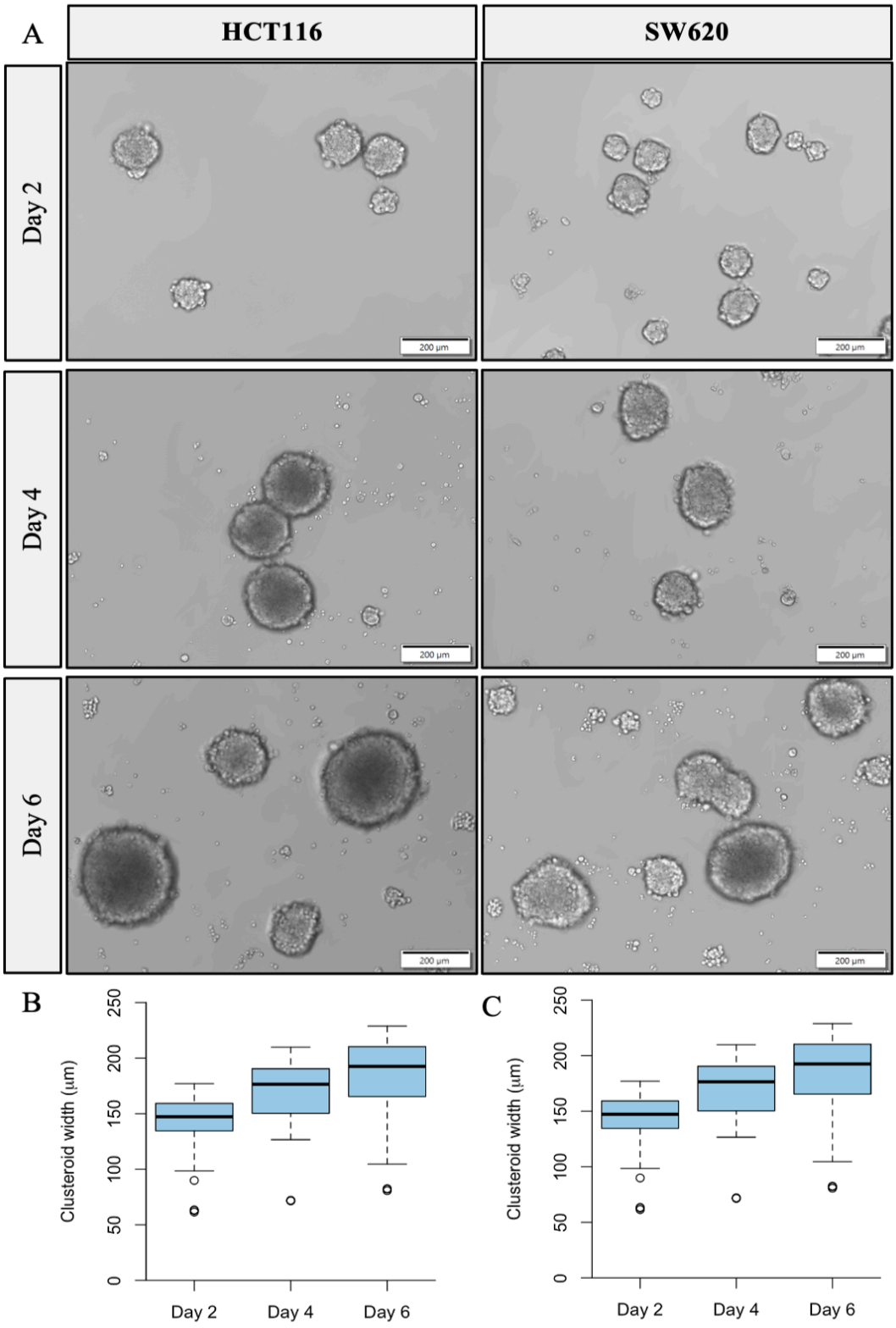

Figure 9. Growth dynamics of 3D clusteroids formed by HCT116 and SW620 cells over time. (A) Representative brightfield images of clusteroids formed by HCT116 (left) and SW620 (right) cells on Days 2, 4, and 6 of culture duration. Progressive increases in clusteroid size and compactness are visible across both cell lines. Scale bars: 200 µm. (B–C) Quantitative measurement of clusteroid width over time: (B) HCT116, (C) SW620.

4.3 Evaluation of ATO/D-VC combination in 3D cell cultures

Following 48-hour exposure to ATO (7.5 μM), D-VC (1.5 mM), or their combination, HCT116 and SW620 clusteroids were evaluated for both morphological and functional changes. Brightfield microscopy revealed that clusteroids maintained their compact and spherical morphology under ATO and D-VC single-drug treatments, with little visible deviation from the untreated controls (Figures 10A–C and 11A–C). However, under ATO/D-VC treatment (Figures 10D and 11D), slight peripheral cell disintegration and mild loosening of the clusteroid structure were observed, suggesting a modest degree of structural compromise.

Quantitative analysis of clusteroid average size (Figures 10E and 11E) showed a subtle reduction in clusteroid width in the ATO/D-VC group compared to the control and single-agent groups, suggesting a minimal inhibitory effect on 3D clusteroid growth. While ATO and D-VC did not significantly affect clusteroid growth, the combination appeared to suppress size increase, particularly in SW620 clusteroids, which showed greater sensitivity. This trend is additionally illustrated in Supplementary Figures A3 and A4, which present the clusteroid size distributions before and after treatment as histograms, based on the same dataset.

Analysis by MTS proliferation assay (Figures 10F and 11F) confirmed the limited impact of single-drug treatments and the moderate effect of the ATO/D-VC combination in 3D clusteroids. In HCT116 clusteroids, ATO/D-VC treatment reduced metabolic activity from 100% in the control group to approximately 85%, corresponding to a reduction of about 1.18-fold. In SW620 clusteroids, the decrease was more pronounced, from 100% to around 60%, indicating a roughly 1.7-fold reduction. These results point to a stronger antiproliferative response in the SW620 line, while the effect in HCT116 remained modest.

Hoechst/PI viability analysis (Figures 10G and 11G) revealed a comparable trend. In HCT116 clusteroids, viability decreased from about 96% in the control to 86% after treatment, amounting to an approximate 1.1-fold reduction. In SW620 clusteroids, cell viability dropped from 96% to around 82%, reflecting a roughly 1.2-fold decrease. While the overall cytotoxic response was moderate, these findings support a synergistic effect of the ATO/D-VC combination, particularly in SW620 clusteroids, and underscore the higher drug resistance of 3D culture models. Despite the enhanced resistance of the 3D models, these findings confirm that, similar to 2D cultures, the combination of ATO and D-VC exhibits a synergistic yet moderate cytotoxic effect in 3D clusteroids.

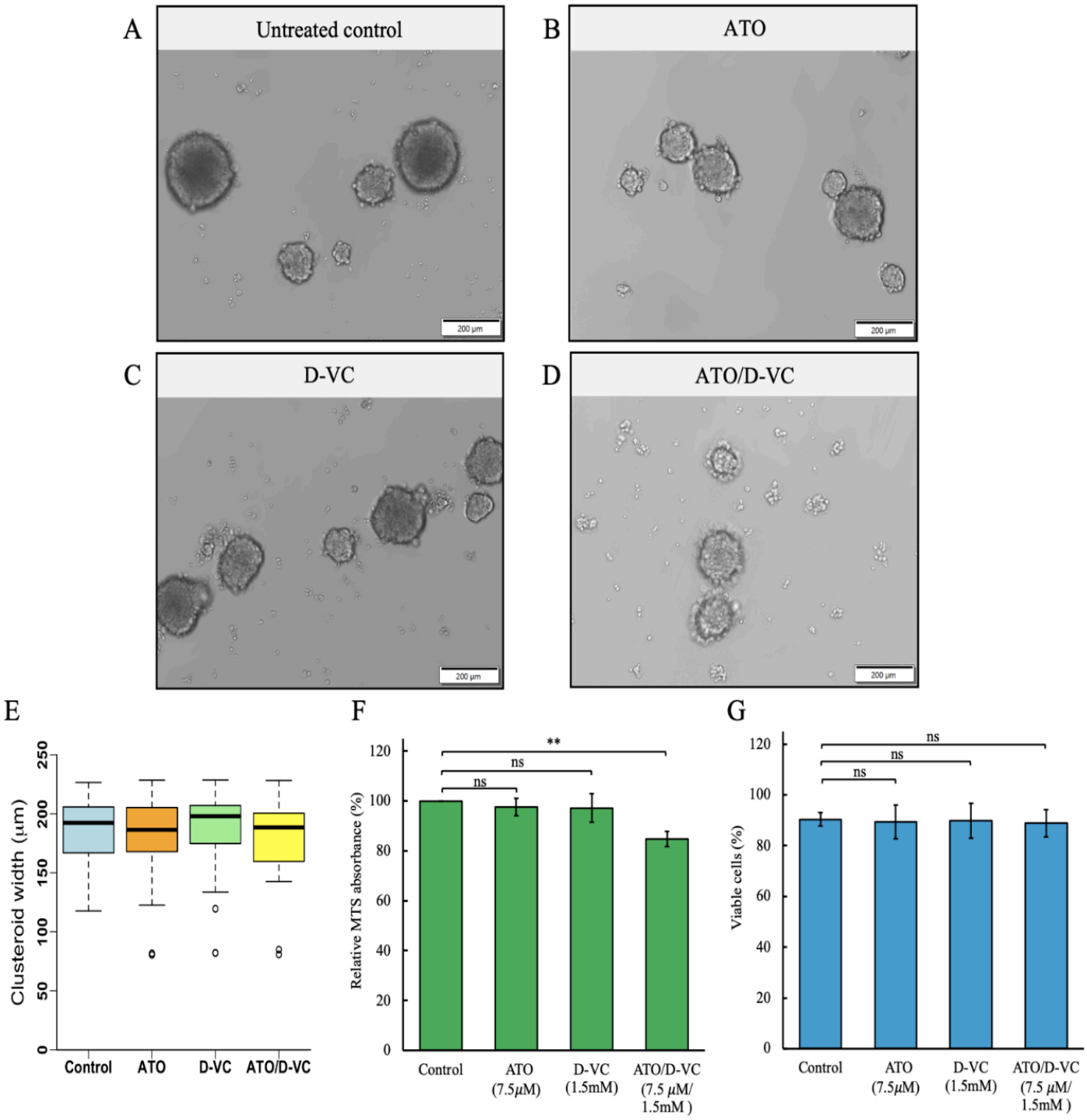

Figure 10. Effect of oxidative drug combinations on HCT116 clusteroids. (A–D) Representative brightfield images of HCT116 clusteroids after 48-hour treatment: (A) Untreated control; (B) ATO (7.5 µM); (C) D-VC (1.5 mM); (D) ATO/D-VC combination (7.5 µM / 1.5 mM). Scale bars: 200 µm. (E) Clusteroid width measured after treatment across all conditions (n = 90 clusteroids per condition from three independent experimental replicates); (F) Cell proliferation measured by MTS assay; (G) Cell viability assessed via Hoechst/PI assay. Data represent mean ± SD from three independent biological replicates performed in technical triplicates. Statistical comparisons were performed using unpaired, two-tailed Student's t-tests with Bonferroni correction. Statistical significance is indicated as follows: ns = not significant; **$p < 0.01$.

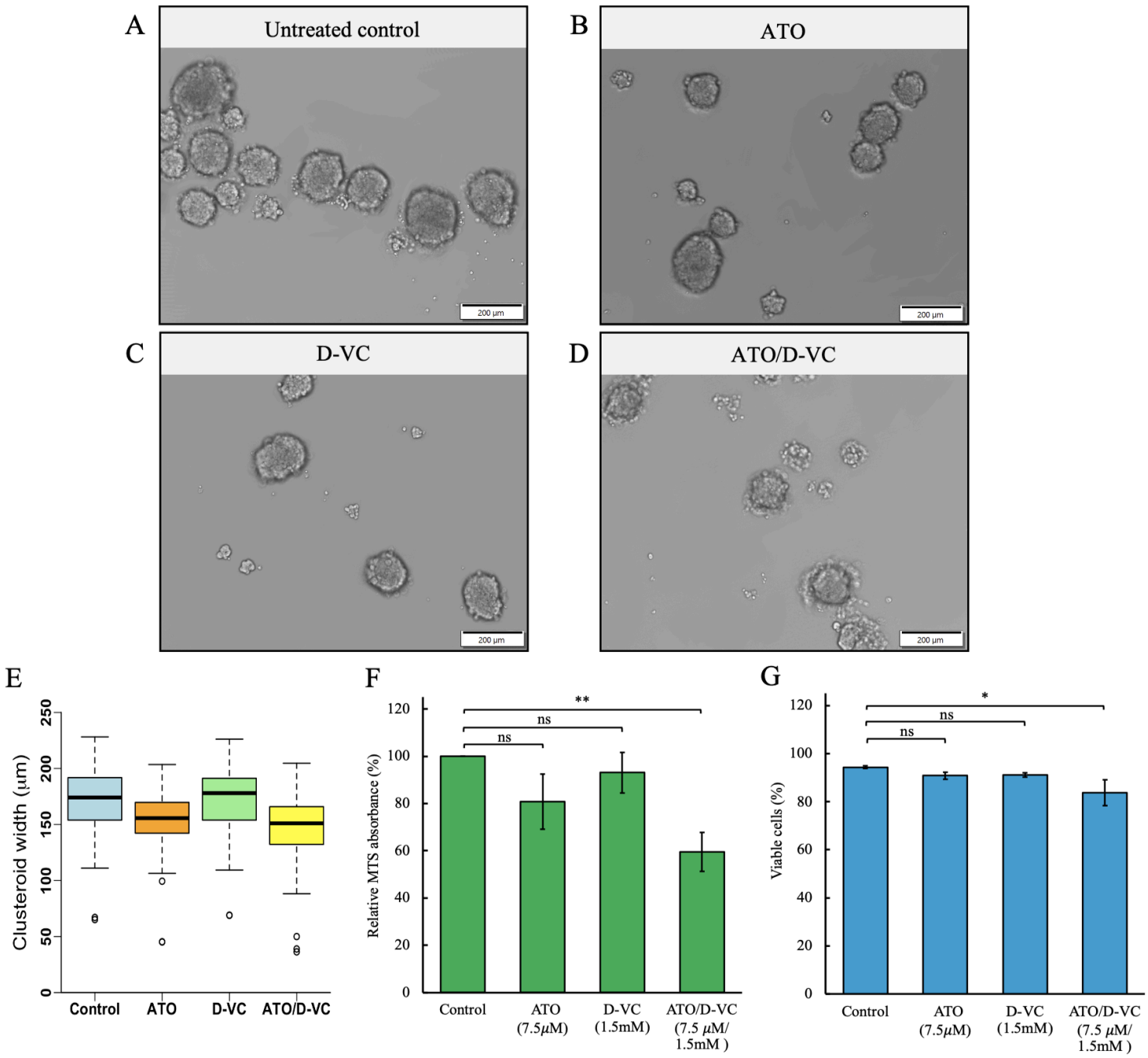

Figure 11. Effect of oxidative drug combinations on SW620 clusteroids. (A–D) Representative brightfield images of SW620 clusteroids after 48-hour treatment: (A) Untreated control; (B) ATO (7.5 µM); (C) D-VC (1.5 mM); (D) ATO/D-VC combination (7.5 µM / 1.5 mM). Scale bars: 200 µm. (E) Clusteroid width measured after treatment across all conditions (n = 90 clusteroids per condition from three independent experimental replicates); (F) Cell proliferation measured by MTS assay; (G) Cell viability assessed via Hoechst/PI assay. Data represent mean ± SD from three independent biological replicates performed in technical triplicates. Statistical comparisons were performed using unpaired, two-tailed Student's t-tests with Bonferroni correction. Statistical significance is indicated as follows: ns = not significant; *p < 0.05; **p < 0.01.

4.4 Comparative analysis of drug response in 2D vs. 3D culture models

To directly compare treatment efficacy between 2D and 3D cell cultures, previously shown data (Figures 6, 7, 10, and 11) were combined in Figure 12 to allow a head-to-head comparison. Across both HCT116 and SW620 cell lines, the ATO/D-VC combination demonstrated significantly greater efficacy in 2D cultures, where the reduction in proliferation was more than twice that observed in 3D culture. In HCT116 cells, proliferation inhibition in 2D was over two-fold higher than in 3D, while in SW620 cells, the difference approached two-fold as well ($p < 0.001$ and $p < 0.01$, respectively). A similar trend was observed for cell viability: 2D cultures showed nearly twofold greater decreases in viable cell percentages compared to their 3D counterparts ($p < 0.001$ for both cell lines). These results underscore a marked difference in treatment response between the two models, highlighting the greater resistance of the cells in 3D culture to oxidative drug therapy. The untreated control and single-drug groups maintained relatively high viability and proliferation in both formats, with noticeable effects observed only upon combination treatment. Overall, clusteroids retained higher metabolic activity and viability than 2D cultures under identical drug exposure conditions (Figure 12).

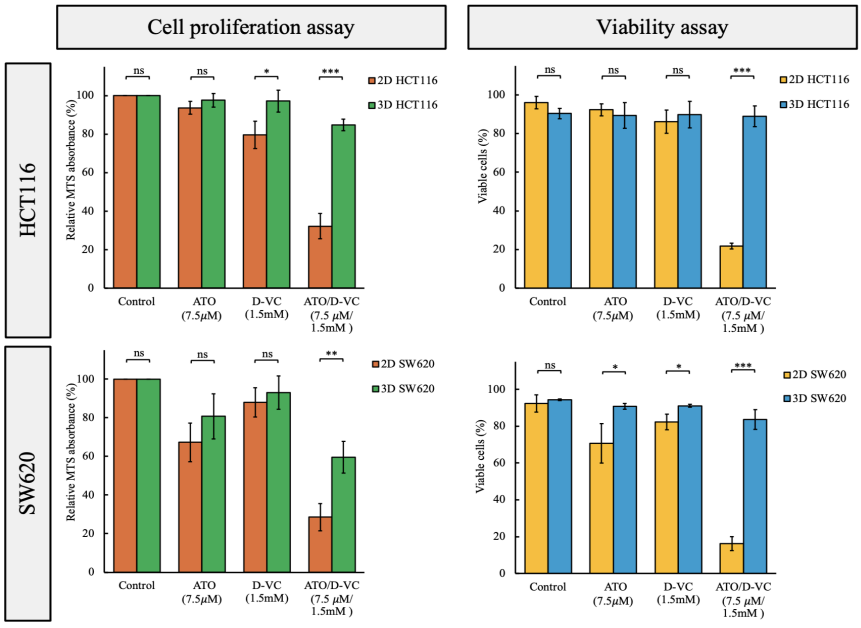

Figure 12. Comparison of 2D and 3D responses to oxidative drug treatments in HCT116 and SW620 cells. Cell proliferation (left) and viability (right) assays performed after 48-hour treatment with ATO (7.5 μM), D-VC (1.5 mM), or ATO/D-VC combination (7.5 μM / 1.5 mM) in 2D and 3D culture models. Top row: HCT116; bottom row: SW620. Data represent mean ± SD from three independent biological replicates performed in technical triplicates. Statistical comparisons were performed using unpaired, two-tailed Student's t-tests. Statistical significance is indicated as follows: ns = not significant; *p < 0.05; **p < 0.01; ***p < 0.001.

4.5 Nanoparticle characterization and coating with Savinase

Physicochemical characterization of the nanoparticles was done to optimize the pH conditions and the Savinase concentration required for efficient surface coating. Zeta potential analysis of uncoated nanoparticles and free Savinase across a range of pH values revealed that pH 5 provided the most favorable electrostatic conditions for coating. At this pH, Savinase carried a strong positive charge (+15 mV), while the nanoparticles maintained a sufficiently high negative surface charge (−19 mV), facilitating strong electrostatic attraction between the cationic Savinase and the NPs surface (Figure 13A).

Following coating, zeta potential measurements showed a gradual increase in surface charge with increasing Savinase concentrations, reaching a plateau at approximately 0.5–0.6 wt% (Figure 13B), suggesting saturation of surface binding sites. In parallel, particle hydrodynamic diameter increased upon coating with higher Savinase concentrations (Figure 13C), supporting successful surface deposition of the enzyme.

Based on the data in Figure 13B–C, 0.6 wt% was selected as the optimal Savinase coating concentration to ensure maximal surface charge. SEM imaging of nanoparticles prepared at this concentration and loaded with either ATO or D-VC confirmed well-defined surface structure and morphology (Figure 13D–E). The average particle size observed by SEM was approximately 190–200 nm, based on direct measurements in the same images. This size is consistent with the hydrodynamic diameter measured by DLS at the same coating level (~270 nm; Figure 13C), further supporting the validity of the formulation strategy. The slightly smaller size observed in SEM can be attributed to the drying of samples during preparation, which results in a more compact appearance of the particles.

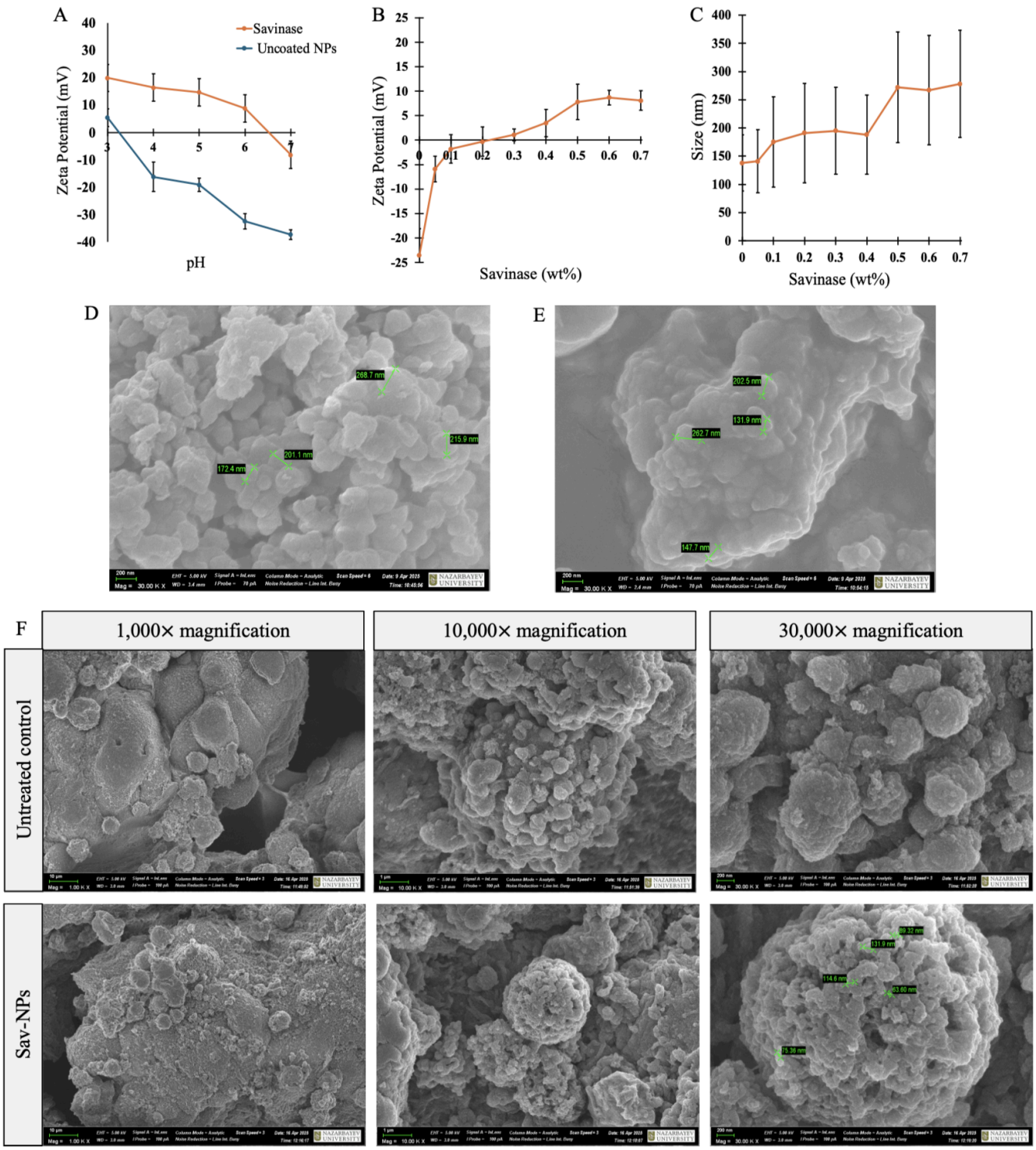

Figure 13. Physicochemical characterization of nanoparticles and Savinase coating. (A) Zeta potential of Savinase and uncoated NPs across pH. (B–C) Zeta potential and hydrodynamic size of Savinase-coated NPs at varying coating concentrations. (D–E) SEM images of Savinase-coated NPs loaded with ATO (D) and D-VC (E). (F) SEM comparison of untreated (top) and Savinase-NP-treated (bottom) 3D HCT116 cells at 1,000×, 10,000×, and 30,000× magnification. Treated cells display surface-bound nanoparticles (63–132 nm), absent in controls. Data in (B) and (C) are from unloaded NPs and shown as mean ± SD (n = 2, 50 DLS runs per replicate).

To evaluate whether Sav-NPs were able to adsorb to the surface of cancer cells, SEM imaging was performed on HCT116 cells grown in 3D cell culture. Untreated control cells and cells incubated with unloaded Sav-NPs were imaged at three magnifications (1,000×, 10,000×, and 30,000×) from the same region to capture both overall structure and nanoscale surface morphology (Figure 13F). In untreated control cells, the surface appeared relatively smooth or folded, with no nanoscale spherical features detected even at the highest magnification. In contrast, Savinase-NP-treated cells exhibited a roughened membrane surface, with clearly distinguishable, uniformly distributed spherical structures attached ranging from 63 to 132 nm—consistent with the size and shape of the nanoparticles (Figure 13C-E). These results confirm successful surface localization of the coated nanoparticles on the HCT116 cells walls in the clusteroids. At present SEM images can only confirm the presence of the particles on the peripheral cells of the clusteroids. Additional experiments are ongoing to confirm nanoparticle penetration in the core of the clusteroids by using fluorescent tracers.

4.6 Evaluation of Savinase-coated nanoparticles (Sav-NPs) in 3D clusteroids

To assess the efficacy of nanoparticle-mediated delivery of oxidative drugs, HCT116 and SW620 clusteroids were treated with ATO and D-VC (7.5 μM / 1.5 mM) delivered in different formulations, including free drugs, Savinase-coated unloaded nanoparticles, and several Savinase-coated nanoparticle (Sav-NPs) combinations. The tested formulations included: Sav-ATO NPs (Savinase-coated nanoparticles loaded with ATO), Sav-D-VC NPs (Savinase-coated nanoparticles loaded with D-VC), Sav-ATO NPs with free D-VC (ATO-loaded Savinase-coated nanoparticles co-administered with free D-VC), and Sav-ATO & Sav-D-VC NPs (a combination of two types of Savinase-coated nanoparticles, each separately loaded with ATO or D-VC, delivered together). Representative brightfield images (Figures 14A–F and 15A–F) illustrate the morphological impact of each treatment condition.

In the untreated control and Savinase-coated unloaded NP groups, clusteroids retained their spherical morphology with minimal disruption. Treatment with either Sav-ATO or Sav-D-VC NPs caused partial clusteroid loosening and decreased compactness. These effects were more pronounced when both agents were delivered together, either as a mixed formulation (Sav-ATO NPs with free D-VC) or as dual-loaded nanoparticles (Sav-ATO & Sav-D-VC NPs).

In these latter groups, clusteroids appeared highly fragmented and disintegrated, particularly in SW620 cultures, where dense scattering of cells was observed.

Quantitative MTS assay results (Figures 14G and 15G) confirmed these observations. In both HCT116 and SW620 clusteroids, treatment with Sav-ATO & Sav-D-VC nanoparticles resulted in the greatest reduction in cell proliferation, decreasing levels to approximately 45% and 35% of control values, respectively. This corresponds to an approximate 2.2-fold reduction in HCT116 and a nearly 2.9-fold reduction in SW620, relative to untreated controls. The group treated with Sav-ATO NPs in combination with free D-VC also exhibited substantial suppression of cell proliferation, with a reduction of about 1.7-fold in HCT116 and around 2.2-fold in SW620. Single-agent nanoparticle groups (Sav-ATO NPs and Sav-D-VC NPs) produced more modest effects, with reductions ranging from 1.4- to 1.6-fold compared to control. In contrast, unloaded Savinase-coated nanoparticles had minimal impact on cell proliferation, confirming the biocompatibility of the nanoparticle carrier itself.

Hoechst/PI viability assay data (Figures 14H and 15H) showed a parallel trend. Clusteroids treated with the combination of separately encapsulated Savinase-coated ATO and D-VC nanoparticles (Sav-ATO & Sav-D-VC NPs) exhibited the most significant drop in viability. In SW620 clusteroids, viability decreased from approximately 95% in the control to around 33%, representing a nearly threefold reduction. In HCT116 clusteroids, viability dropped from about 94% to roughly 45%, indicating a more than twofold decrease.

Other formulations, including Sav-ATO NPs, Sav-D-VC NPs, and the combination of Sav-ATO NPs with free D-VC, produced intermediate reductions, with viability levels falling to approximately 60–75% of the control. Importantly, unloaded Savinase-coated nanoparticles had minimal impact on cell proliferation and viability, maintaining values close to untreated controls in both models. This indicates that the Savinase coating of empty NPs does not induce their cytotoxicity, supporting its use as a biocompatible delivery platform. These results suggest that Savinase-functionalized nanoparticles serve as an effective carrier system, enabling drug penetration and release within cell clusteroid structures without compromising baseline cell health.

Altogether, both assays demonstrated that the dual Savinase-coated nanoparticle treatment resulted in the strongest reduction of cell proliferation and viability across all tested formulations.

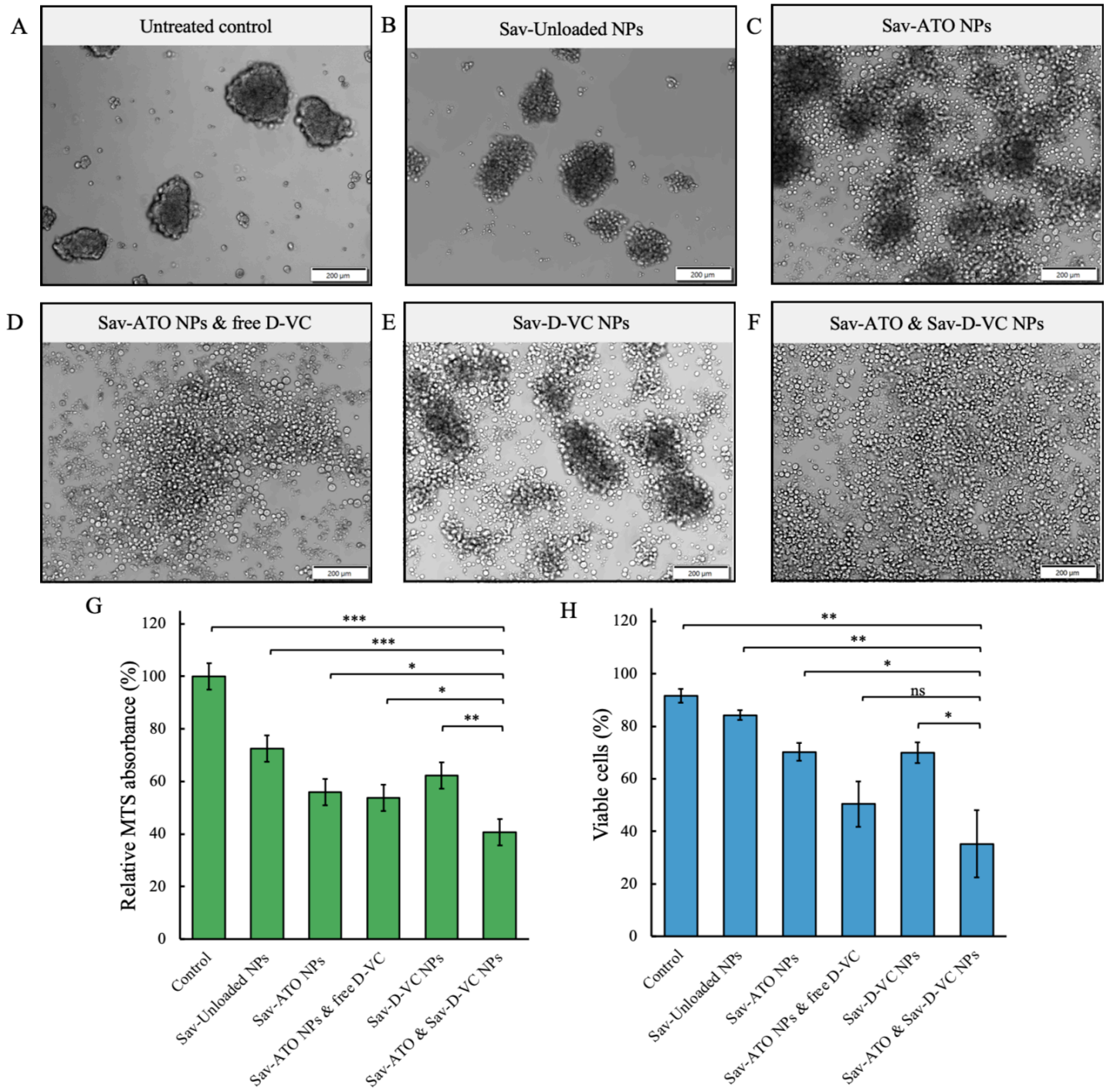

Figure 14. Effect of Savinase-coated nanoparticle formulations on HCT116 clusteroids. (A–F) Brightfield images of HCT116 clusteroids after 48-hour treatment with ATO/D-VC (7.5 µM / 1.5 mM) delivered in various formulations: (A) Untreated control; (B) Sav-coated unloaded NPs; (C) Sav-ATO NPs; (D) Sav-ATO NPs with free D-VC; (E) Sav-D-VC NPs; (F) Sav-ATO & Sav-D-VC NPs. Scale bars: 200 µm. (G) Cell proliferation measured by MTS assay; (H) Cell viability assessed via Hoechst/PI assay. Data represent mean ± SD from three independent biological replicates performed in technical triplicates. Statistical comparisons were performed using unpaired, two-tailed Student's t-tests with Bonferroni correction. Statistical significance is indicated as follows: ns = not significant; *$p < 0.05$; **$p < 0.01$; ***$p < 0.001$.

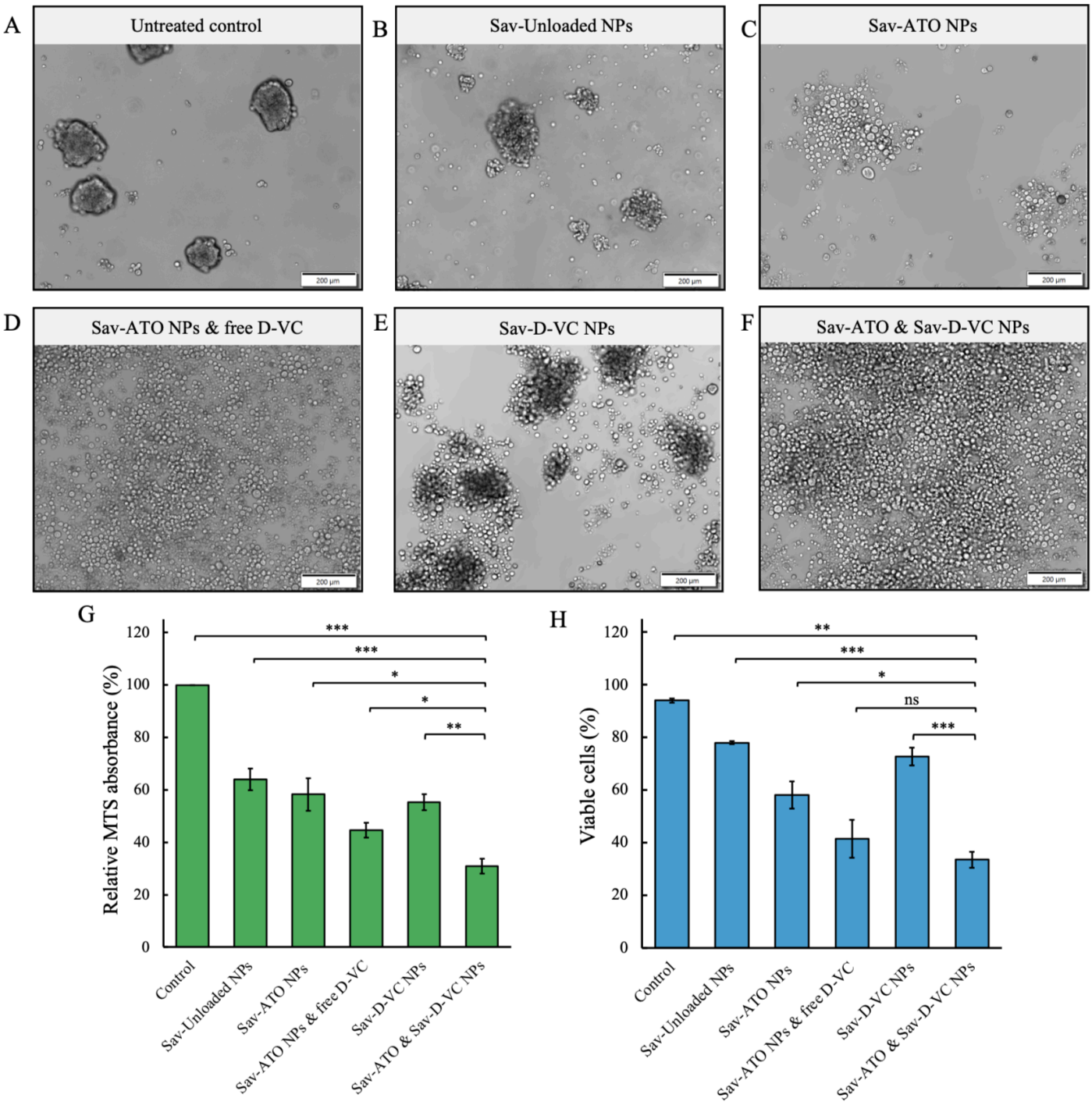

Figure 15. Effect of Savinase-coated nanoparticle formulations on SW620 clusteroids. (A–F) Brightfield images of SW620 clusteroids after 48-hour treatment with ATO/D-VC (7.5 μM / 1.5 mM) delivered in various formulations: (A) untreated control; (B) Savinase-coated unloaded NPs; (C) Sav-ATO NPs; (D) Sav-ATO NPs with free D-VC; (E) Sav-D-VC NPs; (F) Sav-ATO & Sav-D-VC NPs. Scale bars: 200 μm. (G) Cell proliferation measured by MTS assay; (H) Cell viability assessed via Hoechst/PI assay. Data represent mean ± SD from three independent biological replicates performed in technical triplicates. Statistical comparisons were performed using unpaired, two-tailed Student's t-tests with Bonferroni correction. Statistical significance is indicated as follows: ns = not significant; *$p < 0.05$; **$p < 0.01$; ***$p < 0.001$.

3.7 Comparative efficacy of oxidative drug delivery strategies

Figure 16 presents a direct comparison of oxidative drug formulations in HCT116 and SW620 clusteroids. For this analysis, data for the Savinase-coated ATO & D-VC nanoparticles, previously shown in Figures 14 and 15, were combined with additional conditions: free ATO/D-VC and uncoated ATO & D-VC nanoparticles. Although these conditions are displayed separately in Figure 16 for clarity, all treatments were conducted within the same experimental set, using the same biological replicates to ensure consistency across comparisons. The combined dataset in Figure 16 enables head-to-head evaluation of the cytotoxic efficacy of different delivery formulations under identical conditions.

In both HCT116 and SW620 clusteroids, the Savinase-coated dual-drug formulation resulted in the most substantial reduction in proliferation, as shown by the MTS assay (Figure 16, left panels). Free ATO/D-VC caused a greater decrease in metabolic activity and proliferation than uncoated NPs in both cell lines, with this effect being especially pronounced in SW620. In contrast, uncoated NPs led to only moderate suppression compared to the control, suggesting less efficient drug delivery or uptake in 3D spheroids.

The cell viability assay data (Figure 16, right panels) mirrored these trends. Free ATO/D-VC again produced a more noticeable decline in the percentage of viable cells than uncoated NPs, while Savinase-coated NPs led to the most dramatic reduction across both models. Control groups maintained high viability, and no significant changes were observed in the absence of the drug treatment.Together, these results demonstrate a stepwise increase in efficacy across delivery formats, with Sav-NPs achieving the strongest suppression of proliferation and viability in 3D colorectal cancer culture model.

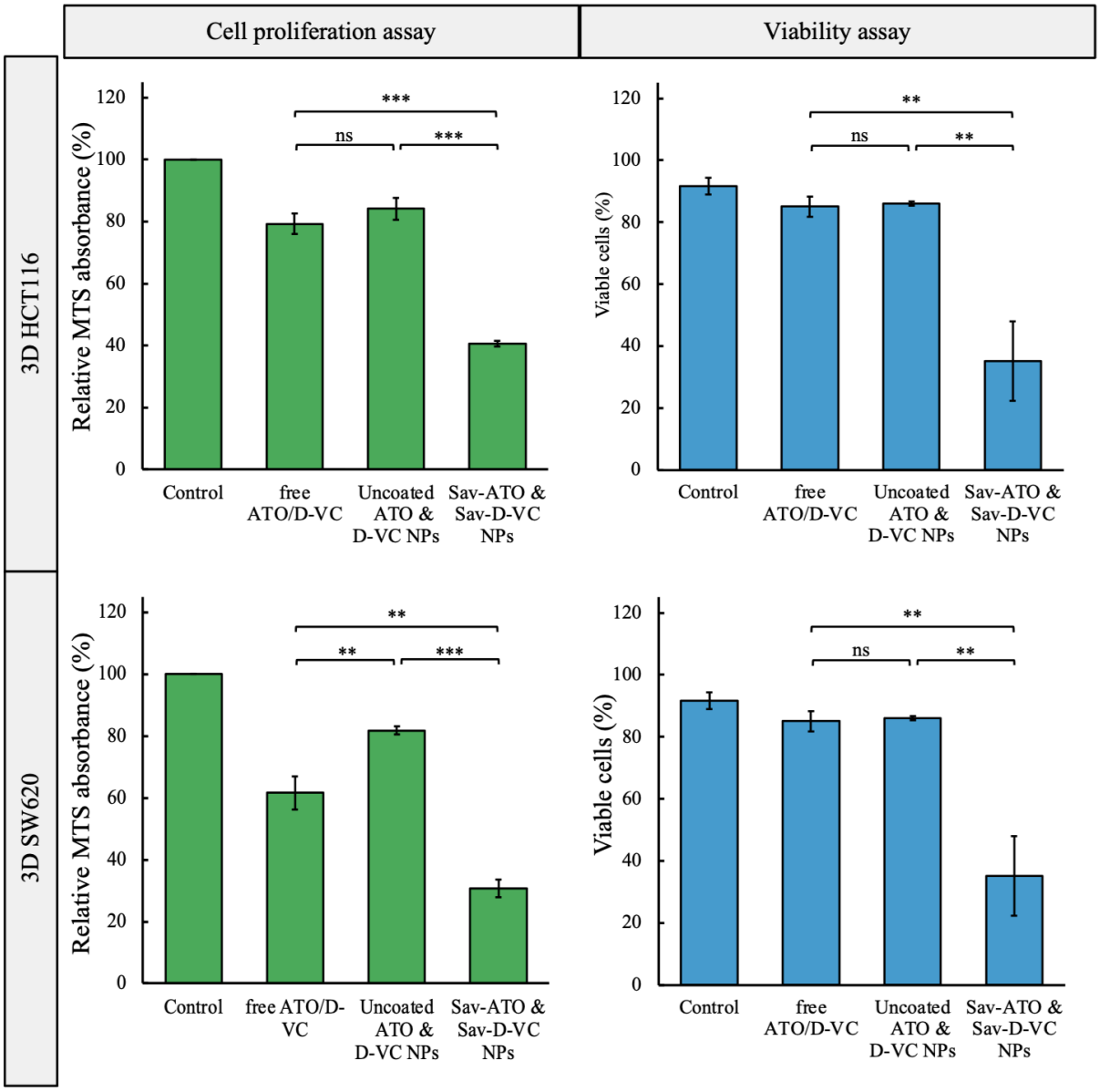

Figure 16. Comparison of oxidative drug formulations in 3D clusteroids of HCT116 and SW620 cells. Cell proliferation (left) and viability (right) assays in HCT116 (top row) and SW620 (bottom row) clusteroids after 48-hour treatment with ATO/D-VC (7.5 μM / 1.5 mM) delivered as free drugs, uncoated nanoparticles, or Savinase-coated nanoparticles. Data represent mean ± SD from three independent biological replicates performed in technical triplicates. Statistical comparisons were performed using unpaired, two-tailed Student's t-tests with Bonferroni correction. Statistical significance is indicated as follows: ns = not significant; *p < 0.05; **p < 0.01; ***p < 0.001.

5 DISCUSSION

This study aimed to investigate two primary hypotheses: (i) that the oxidative combination of arsenic trioxide (ATO) and D-vitamin C (D-VC) would demonstrate reduced cytotoxicity in 3D CRC cell models compared to conventional 2D cell cultures, due to ECM–mediated diffusion barriers and limited drug penetration, and (ii) that encapsulation of ATO and D-VC into Savinase-coated shellac–poloxamer nanoparticles (Sav-NPs) would enhance the therapeutic effect of the oxidative drug combination in 3D cell cultures by improving ECM penetration and drug accessibility to inner cell layers (Section 3). The experimental findings confirmed both assumptions and further extended current understanding of oxidative drug delivery systems in solid tumor models.

5.1 Model-dependent differences in treatment responsiveness

Consistent with expectations, the oxidative combination of ATO and D-VC induced greater cytotoxic effect in 2D monolayers compared to 3D CRC cell cultures. In both HCT116 and SW620 cell lines, clusteroids exhibited minimal responsiveness, likely due to the presence of the ECM, which serves as a physical barrier that restricts drug access to inner cell layers [8–10]. This differential treatment outcome was clearly illustrated in Figure 12, where the same drug concentrations produced a stronger suppression of cell proliferation and viability in 2D conditions, while the effect in 3D culture model remained comparatively weak. These results demonstrate the importance of incorporating 3D cell model testing when evaluating therapeutic efficacy, particularly for solid tumor–targeted interventions.

The observed trend is consistent with previous findings in cell spheroid systems derived from breast and pancreatic cancers, where limited drug diffusion has similarly led to underestimation of treatment effectiveness in traditional 2D assays [9]. These parallels further validate the clusteroid model as a physiologically relevant platform for analyzing drug resistance capability.

Moreover, although overall sensitivity was reduced in cell clusteroids, the synergistic interaction between ATO and D-VC was preserved once the drugs reached their intracellular targets. The combination outperformed either agent alone, indicating that the synergistic effect of ATO and D-VC is retained in 3D models once the drugs reach their targets. In 2D cell monolayers, treatment with ATO, D-VC, and their combination produced responses consistent

with previous studies [5, 7], confirming a pronounced synergistic effect relative to monotherapies (Figures 6 and 7).

It is important to note that the reduced susceptibility of clusteroids does not indicate treatment failure but rather reflects the limitations of single-dose exposure. In clinical and preclinical studies of tumor therapy, repeated dosing is commonly employed to achieve sustained therapeutic effects. Nanoparticle encapsulation may help address this limitation by enhancing local bioavailability and reducing the frequency and duration of treatment.

Together, these findings highlight the critical influence of dimensional context on drug efficacy and support the growing implementation of 3D models in preclinical testing.

5.2 Therapeutic advantages of Savinase-functionalized nanoparticles

Encapsulation of ATO and D-VC into Savinase-coated shellac–poloxamer nanoparticles (Sav-NPs) significantly enhanced cytotoxic outcomes in 3D cell cultures compared to both free drug combinations and uncoated nanoparticle formulations. This improvement in therapeutic effect appears to result from a combination of enzymatic interaction with the clusteroid microenvironment and favorable electrostatic adhesion conferred by the Savinase coating.

Although ECM composition was not directly characterized, the morphological changes observed in brightfield images, particularly the fragmentation of clusteroids in the Sav-ATO & Sav-D-VC NP group (Figures 14F and 15F), suggest that the presence of the Savinase coating may have contributed to partial disintegration of the clusteroid surface. Given Savinase's proteolytic nature, its surface coating could have facilitated localized softening of the outer matrix, hence improving nanoparticle access to deeper cell layers in the clusteroids cores. This interpretation parallels prior reports involving lysozyme- and Alcalase-coated nanoparticles, which enhanced penetration through dense biological matrices such as biofilms and tissue spheroids [16].

Additionally, the cationic nature of the coating with Savinase, confirmed through zeta potential analysis (Figure 13B), likely enhances nanoparticle deposition on the negatively charged cancer cell membranes. This electrostatic interaction may improve both surface retention and internalization. SEM imaging of HCT116 clusteroids treated with Sav-NPs further demonstrated the presence of spherical particles adherent to the cell surface (Figure 13F), demonstrating the successful targeting. However, it should be noted that SEM imaging confirms

particle presence only on peripheral cells of the clusteroids. It is important to note that SEM imaging currently provides evidence of nanoparticle localization only at the clusteroid periphery. Ongoing experiments with fluorescent tracers are being conducted to evaluate whether the nanoparticles can also penetrate into the inner regions of the 3D structures.

The enhanced performance of Savinase-functionalized nanoparticles across both colorectal cancer models highlights the therapeutic benefit of delivering ATO and D-VC as encapsulated into nanoparticles, surface-functionalized formulations. The combined application of Sav-ATO and Sav-D-VC nanoparticles resulted in the most pronounced treatment response, consistent with the proposed mechanism involving improved penetration and surface targeting within 3D clusteroids. This outcome, supported by cell viability and proliferation assays (Figures 14–16), reinforces the importance of combining enzymatic surface activity with dual-agent delivery to address the diffusion barriers characteristic of dense tumor-like structures.

5.3 Comparison with contemporary nanocarrier approaches

The observed benefits of Sav-NPs are consistent with broader trends in nano-oncology, which increasingly employ surface-modified nanocarriers to enhance barrier penetration across diverse applications, including tumor ECM, bacterial biofilms, and intracellular organelles [11, 13, 14, 16]. Unlike mitochondria-targeted nanocarriers that depend on synthetic moieties such as triphenylphosphonium [13], the Savinase-coated shellac–poloxamer system is based on biocompatible materials and incorporates a clinically used enzyme, supporting its translational potential. This aligns with emerging perspectives in the field that emphasize biocompatibility and functional versatility for future clinical applications [15].

5.4 Observations regarding uncoated nanoparticle performance

An unexpected observation was the reduced cytotoxicity upon treatment with uncoated ATO/D-VC nanoparticles compared to the free-drug formulation at 48 hours. This may be explained by incomplete or delayed release of encapsulated drugs from the shellac matrix, a phenomenon similarly noted in metformin-loaded lysozyme-coated particles under suboptimal coating conditions [14]. These results highlight a critical balance between nanoparticle stability and drug release kinetics: excessive matrix integrity can hinder timely drug availability, while insufficient stability may reduce retention at the target site.

5.5 Limitations of the study

Several limitations should be acknowledged. First, drug encapsulation efficiency and release kinetics for ATO and D-VC were not directly measured; instead, absolute encapsulation and complete release over 48 hours were assumed based on the initial formulation parameters. Preliminary attempts to perform high-performance liquid chromatography (HPLC) analysis of th NP supernatant were made, but access to instrumentation was limited during the study period. This analysis is ongoing and will be included in a paper manuscript currently in preparation. Future studies involving HPLC and dialysis assays are required to accurately quantify encapsulation efficiency, characterize drug release kinetics, and evaluate delivery performance, which will be essential for refining dosing models. Second, the ECM composition of the clusteroids, such as collagen, fibronectin, or matrix stiffness, was not characterized. Since these factors are known to influence drug diffusion [8], subsequent investigations should include biochemical and mechanical profiling of the clusteroid matrix to evaluate how Savinase alters its structure. The results may impact the choice of alternative more specialized proteases in follow up studies.

5.6 Future directions

Following the promising *in vitro* results presented here, future work will focus on *in vivo* evaluation of Sav-NP pharmacokinetics, biodistribution, tumor penetration, and therapeutic efficacy using animal models of colorectal cancer. Further refinement of the nanoparticle system will include optimizing Savinase coating levels, adjusting shellac crosslinking to balance particle stability with controlled drug release, and refining ATO and D-VC concentrations based on HPLC and dialysis data. Combining real-time release profiles with ECM profiling and *in vivo* outcomes will support the development of more effective and clinically relevant nanoparticle formulations.

5.7 Conclusion

Overall, this study demonstrates the therapeutic potential of combining oxidative drugs with ECM-digesting, positively charged nanocarriers for improved treatment of KRAS-mutant colorectal cancer. Savinase-functionalized nanoparticles successfully enhanced the cytotoxic

activity of ATO/D-VC in 3D cell culture, exceeding the efficacy of both free drugs and uncoated nanoparticle formulations. By placing these findings in the broader context of oxidative therapies [5, 7], 3D tumor modeling [8–11], and protease-coated nanomedicines [14, 16], the current work contributes to the advancement of clinically applicable nanoformulations for solid tumor therapy.

6 REFERENCES

1. WHO. (2023). *Colorectal cancer*. World Health Organization. https://www.who.int/news-room/fact-sheets/detail/colorectal-cancer
2. Zhu, G., Pei, L., Xia, H., Tang, Q., & Bi, F. (2021). Role of oncogenic kras in the prognosis, diagnosis and treatment of colorectal cancer. *Molecular Cancer*, *20*(1). https://doi.org/10.1186/s12943-021-01441-4
3. Strickler, J. H., Yoshino, T., Stevinson, K., Eichinger, C. S., Giannopoulou, C., Rehn, M., & Modest, D. P. (2023). Prevalence of KRAS G12C mutation and co-mutations and associated clinical outcomes in patients with colorectal cancer: A systematic literature review. *The Oncologist*, *28*(11). https://doi.org/10.1093/oncolo/oyad138
4. Burska, A. N., Ilyassova, B., Dildabek, A., Khamijan, M., Begimbetova, D., Molnár, F., & Sarbassov, D. D. (2022). Enhancing an oxidative "Trojan horse" action of vitamin C with arsenic trioxide for effective suppression of kras-mutant cancers: A promising path at the bedside. *Cells*, *11*(21), 3454. https://doi.org/10.3390/cells11213454
5. Wu, X., Park, M., Sarbassova, D. A., Ying, H., Lee, M. G., Bhattacharya, R., Ellis, L., Peterson, C. B., Hung, M., Lin, H., Bersimbaev, R. I., Song, M. S., & Sarbassov, D. D. (2019). A chirality‐dependent action of vitamin C in suppressing Kirsten rat sarcoma mutant tumor growth by the oxidative combination: Rationale for cancer therapeutics. *International Journal of Cancer*, *146*(10), 2822–2828. https://doi.org/10.1002/ijc.32658
6. Begimbetova, D., Burska, A. N., Baltabekova, A., Kussainova, A., Kukanova, A., Fazyl, F., Ibragimova, M., Manekenova, K., Makishev, A., Bersimbaev, R. I., & Sarbassov, D. D. (2024). The vitamin C enantiomers possess a comparable potency in the induction of oxidative stress in cancer cells but differ in their toxicity. *International Journal of Molecular Sciences*, *25*(5), 2531. https://doi.org/10.3390/ijms25052531
7. Begimbetova, D., Kukanova, A., Fazyl, F., Manekenova, K., Omarov, T., Burska, A. N., Khamijan, M., Gulyayev, A., Yermekbayeva, B., Makishev, A., Saliev, T., Batyrbekov, K., Aitbayev, C., Spatayev, Z., & Sarbassov, D. (2022). The oxidative drug combination for suppressing kras G12D inducible tumour growth. *BioMed Research International*, *2022*, 1–14. https://doi.org/10.1155/2022/9426623

8. Abuwatfa, W. H., Pitt, W. G., & Husseini, G. A. (2024). Scaffold-based 3D cell culture models in cancer research. *Journal of Biomedical Science*, *31*(1). https://doi.org/10.1186/s12929-024-00994-y
9. Kimlin, L. C., Casagrande, G., & Virador, V. M. (2011). In vitro three‐dimensional (3D) models in cancer research: An update. *Molecular Carcinogenesis*, *52*(3), 167–182. https://doi.org/10.1002/mc.21844
10. Wang, A., Madden, L. A., & Paunov, V. N. (2020). Advanced biomedical applications based on emerging 3D cell culturing platforms. *Journal of Materials Chemistry B*, *8*(46), 10487–10501. https://doi.org/10.1039/d0tb01658f
11. Wang, A., Weldrick, P. J., Madden, L. A., & Paunov, V. N. (2021). Biofilm-infected human clusteroid three-dimensional Coculture platform to replace animal models in testing antimicrobial nanotechnologies. *ACS Applied Materials & Interfaces*, *13*(19), 22182–22194. https://doi.org/10.1021/acsami.1c02679
12. Wang, A., Madden, L. A., & Paunov, V. N. (2022). Fabrication of angiogenic sprouting coculture of cell clusteroids using an aqueous two-phase Pickering emulsion system. *ACS Applied Bio Materials*, *5*(4), 1804–1816. https://doi.org/10.1021/acsabm.2c00168
13. Mani, S., Swargiary, G., Tyagi, S., Singh, M., Jha, N. K., & Singh, K. K. (2021). Nanotherapeutic approaches to target mitochondria in cancer. *Life Sciences*, *281*, 119773. https://doi.org/10.1016/j.lfs.2021.119773
14. Wang, A., Madden, L. A., & Paunov, V. N. (2024). Enhanced anticancer effect of lysozyme-functionalized metformin-loaded shellac nanoparticles on a 3D cell model: Role of the nanoparticle and payload concentrations. *Biomaterials Science*, *12*(18), 4735–4746. https://doi.org/10.1039/d4bm00692e
15. Karahmet Sher, E., Alebić, M., Marković Boras, M., Boškailo, E., Karahmet Farhat, E., Karahmet, A., Pavlović, B., Sher, F., & Lekić, L. (2024). Nanotechnology in medicine revolutionizing drug delivery for cancer and viral infection treatments. *International Journal of Pharmaceutics*, *660*, 124345. https://doi.org/10.1016/j.ijpharm.2024.124345
16. Wang, A., Weldrick, P. J., Madden, L. A., & Paunov, V. N. (2021b). Enhanced clearing of *candida* biofilms on a 3D urothelial cell *in vitro* model using lysozyme-functionalized fluconazole-loaded shellac nanoparticles. *Biomaterials Science*, *9*(20), 6927–6939. https://doi.org/10.1039/d1bm01035b

17. Betzel, C., Klupsch, S., Branner, S., & Wilson, K. S. (1996). Crystal structures of the alkaline proteases savinase and esperase from bacillus lentus. *Advances in Experimental Medicine and Biology*, 49–61. https://doi.org/10.1007/978-1-4613-0319-0_7

18. Das, A. A., Filby, B. W., Geddes, D. A., Legrande, D., & Paunov, V. N. (2017). High throughput fabrication of cell spheroids by templating water-in-water pickering emulsions. *Mater. Horiz.*, *4*(6), 1196–1200. https://doi.org/10.1039/c7mh00677b

19. Celik, S. B., Dominici, S. R., Filby, B. W., Das, A. A., Madden, L. A., & Paunov, V. N. (2019). Fabrication of human keratinocyte cell clusters for skin graft applications by templating water-in-water pickering emulsions. *Biomimetics*, *4*(3), 50. https://doi.org/10.3390/biomimetics4030050

20. Wang, A., Madden, L. A., & Paunov, V. N. (2020). High-throughput fabrication of Hepatic Cell clusteroids with enhanced growth and functionality for tissue engineering applications. *Materials Advances*, *1*(8), 3022–3032. https://doi.org/10.1039/d0ma00635a

21. Han, C., Takayama, S., & Park, J. (2015). Formation and manipulation of cell spheroids using a density adjusted PEG/dex aqueous two phase system. *Scientific Reports*, *5*(1). https://doi.org/10.1038/srep11891

22. Tevlek, A., Kecili, S., Ozcelik, O. S., Kulah, H., & Tekin, H. C. (2023). Spheroid engineering in microfluidic devices. *ACS Omega*, *8*(4), 3630–3649. https://doi.org/10.1021/acsomega.2c06052

23. Cacciamali, A., Villa, R., & Dotti, S. (2022). 3d Cell cultures: Evolution of an ancient tool for new applications. *Frontiers in Physiology*, *13*. https://doi.org/10.3389/fphys.2022.836480

24. Urzì, O., Gasparro, R., Costanzo, E., De Luca, A., Giavaresi, G., Fontana, S., & Alessandro, R. (2023). Three-dimensional cell cultures: The bridge between in vitro and in vivo models. *International Journal of Molecular Sciences*, *24*(15), 12046. https://doi.org/10.3390/ijms241512046

25. Weldick, P. J., Wang, A., Halbus, A. F., & Paunov, V. N. (2022). Emerging nanotechnologies for targeting antimicrobial resistance. *Nanoscale*, *14*(11), 4018–4041. https://doi.org/10.1039/d1nr08157h

26. Zhu, M., Wang, P., Chen, B., Shi, L., Long, R., Wang, S., & Liu, Y. (2024). Active-oxygenating hollow Prussian blue nanosystems loaded with biomacromolecules for photodynamic/photothermal therapy of cancer and alleviating hypoxic tumors. *Materials & Design*, *237*, 112618. https://doi.org/10.1016/j.matdes.2023.112618

27. Promega Corporation. (n.d.). *CellTiter 96® AQueous One Solution Cell Proliferation Assay Technical Bulletin*. https://www.promega.com

7 APPENDICES

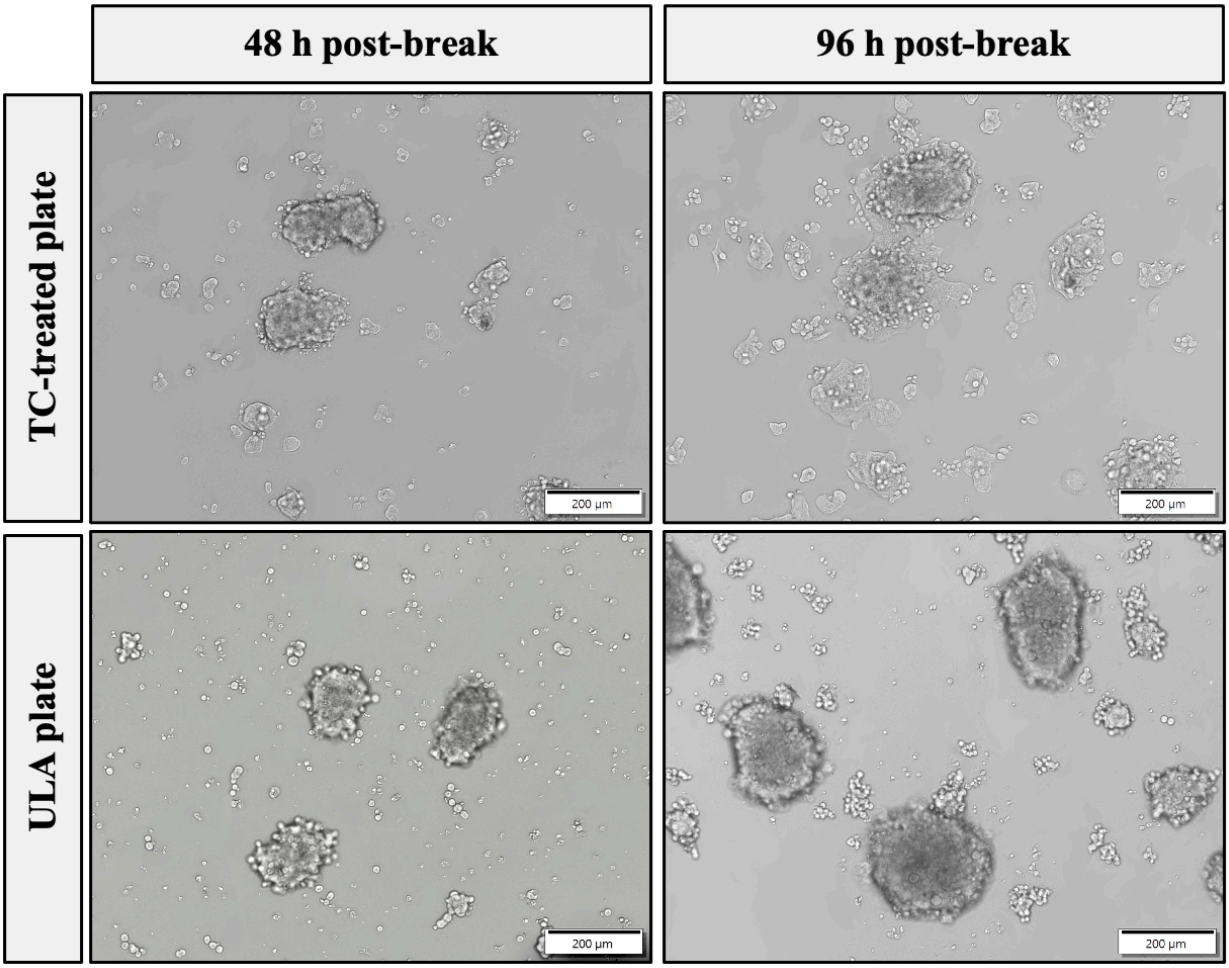

Figure A1. Effect of plate type on clusteroid morphology post-emulsion breakage Representative brightfield images of clusteroids seeded in either TC-treated or ULA (ultra-low attachment) plates and imaged at 48 and 96 hours after emulsion breakage. Scale bars: 200 µm.

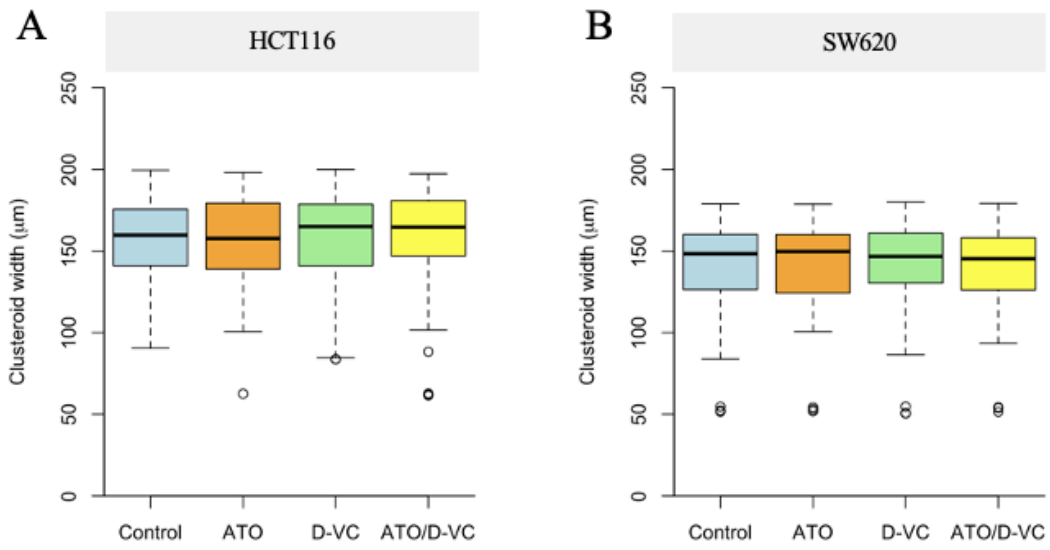

Figure A2. Uniformity of clusteroid size across conditions prior to treatment. (A–B) Box plot analysis of clusteroid width after 48 hours of culture (prior to treatment) for HCT116 (A) and SW620 (B) clusteroids. Conditions include: untreated control, ATO (7.5 µM), D-VC (1.5 mM), and ATO/D-VC combination (7.5 µM / 1.5 mM). Measurements were performed on 90 clusteroids per condition, collected across three experimental replicates.

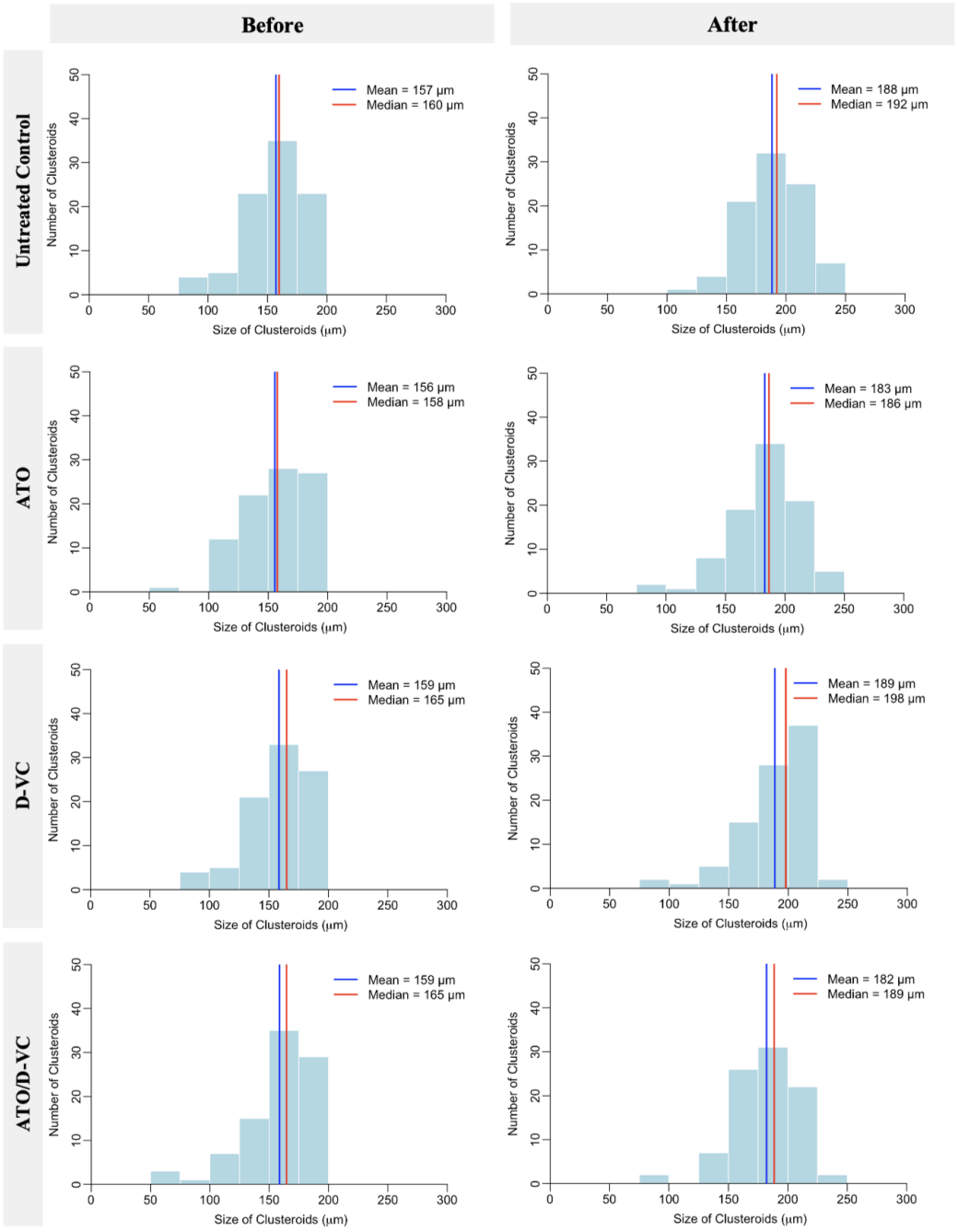

Figure A3. Size distribution of HCT116 clusteroids before and after 48-hour treatment with oxidative drug combinations. Histograms show clusteroid diameters across four treatment groups: untreated control, ATO (7.5 μM), D-VC (1.5 mM), and ATO/D-VC combination (7.5 μM / 1.5 mM). "Before" indicates measurements taken prior to treatment, while "After" represents clusteroid sizes following 48 hours of incubation with the respective conditions. Mean (blue line) and median (red line) values are indicated. Measurements were performed on 90 clusteroids per condition, collected across three independent experimental replicates.

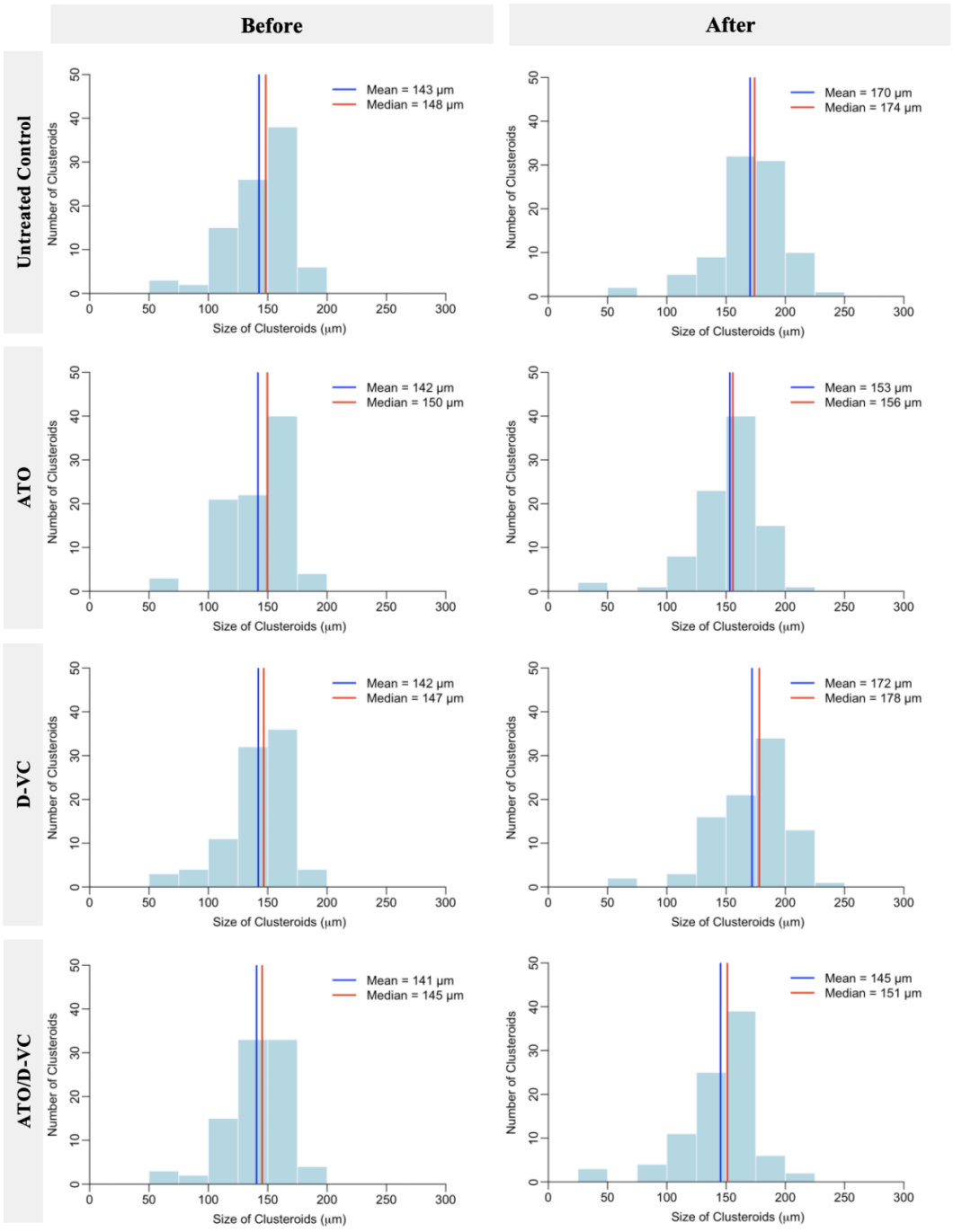

Figure A4. Size distribution of SW620 clusteroids before and after 48-hour treatment with oxidative drug combinations. Histograms show clusteroid diameters across four treatment groups: untreated control, ATO (7.5 µM), D-VC (1.5 mM), and ATO/D-VC combination (7.5 µM / 1.5 mM). "Before" indicates measurements taken prior to treatment, while "After" represents clusteroid sizes following 48 hours of incubation with the respective conditions. Mean (blue line) and median (red line) values are indicated. Measurements were performed on 90 clusteroids per condition, collected across three independent experimental replicates.